Russian Original Vol. 54, No. 6, June, 1983

December, 1983

LL

J.T

File

SATEAZ 54(6) 389–440 (1983)

SOVIET ATOMIC ENERGY

АТОМНАЯ ЭНЕРГИЯ
(ATOMNAYA ÉNERGIYA)

TRANSLATED FROM RUSSIAN

c/b CONSULTANTS BUREAU, NEW YORK

SOVIET ATOMIC ENERGY

Soviet Atomic Energy is abstracted or indexed in *Chemical Abstracts, Chemical Titles, Pollution Abstracts, Science Research Abstracts, Parts A and B, Safety Science Abstracts Journal, Current Contents, Energy Research Abstracts,* and *Engineering Index.*

Mailed in the USA by Publications Expediting, Inc., 200 Meacham Avenue, Elmont, NY 11003.

POSTMASTER: Send address changes to *Soviet Atomic Energy,* Plenum Publishing Corporation, 233 Spring Street, New York, NY 10013.

Soviet Atomic Energy is a translation of *Atomnaya Energiya,* a publication of the Academy of Sciences of the USSR.

An agreement with the Copyright Agency of the USSR (VAAP) makes available both advance copies of the Russian journal and original glossy photographs and artwork. This serves to decrease the necessary time lag between publication of the original and publication of the translation and helps to improve the quality of the latter. The translation began with the first issue of the Russian journal.

Consultants Bureau journals appear about six months after the publication of the original Russian issue. For bibliographic accuracy, the English issue published by Consultants Bureau carries the same number and date as the original Russian from which it was translated. For example, a Russian issue published in December will appear in a Consultants Bureau English translation about the following June, but the translation issue will carry the December date. When ordering any volume or particular issue of a Consultants Bureau journal, please specify the date and, where applicable, the volume and issue numbers of the original Russian. The material you will receive will be a translation of that Russian volume or issue.

Subscription (2 volumes per year)
Vols. 52 & 53: $440 (domestic); $489 (foreign)
Vols. 54 & 55: $500 (domestic); $555 (foreign)

Single Issue: $100
Single Article: $7.50

CONSULTANTS BUREAU, NEW YORK AND LONDON

c/b
233 Spring Street
New York, New York 10013

Published monthly. Second-class postage paid at Jamaica, New York 11431.

SOVIET ATOMIC ENERGY

A translation of *Atomnaya Énergiya*

December, 1983

Volume 54, Number 6 **June, 1983**

CONTENTS

The Russian press date (podpisano k pechati) of this issue was 6/1/1983. Publication therefore did not occur prior to this date, but must be assumed to have taken place reasonably soon thereafter.

ARTICLES

ITERATIVE ALGORITHM FOR OPTIMIZATION OF THE ENERGY DISTRIBUTION IN HIGH-POWERED WATER-COOLED CHANNEL REACTORS (RBMK) WITH THE HELP OF MEASUREMENT OF THE INSERTION DEPTH OF THE SAFETY AND CONTROL RODS (SCR)

A. A. Shkurpelov, V. V. Postnikov,
N. V. Isaev, V. G. Nazaryan, Yu. V. Shmonin,
A. S. Nemirov, and G. V. Yurkin

UDC 621.039.512.45

The problem of profiling the energy distribution arises in the solution of problems of the ongoing operation of a reactor and is associated with providing the initial computational information for the centralized control system (CCS) of the reactor, which is based on the use of a computer. The power W_j of all the heat-generating assemblies (HGA) in a reactor is determined in the system from the readings W_l^d ($l = 1, 2, \ldots, N_d$) of the energy distribution control detectors (EDCD) and from a priori information about the power of the HGA R_j ($j = 1, 2, \ldots, N_{HGA}$) obtained by computational means [1, 2]. Calculations are performed using the two-group two-dimensional diffusion program BOKR [1], in which a quasisteady model of the reactor is employed. In view of the inadequateness of this model for an actual unstable RBMK-1000 reactor, some difficulties associated both with the analysis of the objectivity of the results obtained and with the need for additional correction of the computational data arise in the description of the energy distribution for in-channel control of the power. Taking additional account in the computational model of the dynamic factors has evidently permitted obtaining the macrodistributions reflecting the actual state for an RBMK-1000 in the best case at time intervals up to several minutes. However, calculations using the appropriate programs should take an order of magnitude more time, and therefore the question of performing them in real time can evidently still not be posed.

The approach proposed in this article permits raising the objectivity of the a priori information within the framework of the quasisteady reactor model as a result of taking into account the actions of the nuclear power plant personnel in the extremal regulation of the energy distribution [3]. The use of this information in the plant control system permits limiting the error of determining the power of the channels within permissible limits.

A method for extremal regulation is proposed in the calculations in which the commands for shifting the SCR rods are issued immediately during the iterative process for the nuclear fission soruces in the solution of the diffusion equations. This results in a significant reduction of the computational time (by approximately a factor of 8-10) in comparison with the case in which a program of physical calculation is used as a separate procedure for determination of the system response to shifting of the rods [3].

We shall indicate some distinctive features of the algorithm for recovery of the energy distribution from EDCD readings realized in the PRIZMA program [1, 4] in the "Skala" CCS to explain the method of preparing the a priori information. The assumption that the microstructure of the energy distribution realized in the reactor — the ratio of the power of adjacent channels — is well described by the quasisteady computational model of an RBMK of the BOKR program serves as the basis of the program; this property of the computational model has been confirmed by repeated experiments. Therefore, the recovered power distribution W_j is represented in the form

$$W_j = F_j(1 + V_j), \tag{1}$$

Translated from Atomnaya Énergiya, Vol. 54, No. 6, pp. 387-390, June, 1983. Original article submitted April 26, 1982.

0038-531X/83/5406-0389$07.50

where F_j is a reference distribution calculated from data of the physical computation of R_j and the entire set of readings of the EDCD with the use of the expansion

$$F_j = R_j \sum_{k=1}^{8} C_k \psi_{kj} \tag{2}$$

(here ψ_{kj} are test functions evenly specified for the entire reactor; the coefficients C_k are determined by the least squares method)

$$\sum_{l=1}^{N_d} \left(\frac{W_l^d}{R_l^d} - \sum_{k=1}^{8} C_k \psi_{kl} \right)^2 = \min_{C_k}, \tag{3}$$

where the index d denotes a channel with EDCD, and N_d is the number of EDCD.

The reference distribution F_j is an estimate of the mathematical expectation of the desired energy distribution W_j without taking into account plant estimates of the dispersion of the calibration error of the EDCD. In relationship (1), V_j is the local correction with corrects the estimate F_j with account taken of the four EDCD nearest to the channel under discussion. Its use is justified only in the case in which estimates are known for the dispersion of the calibration error of the EDCD $\sigma^2_{c,l}$. An estimate of V_j is determined by means of a smooth statistical interpolation [4] of the approximate values $V_l^d = W_l^d/F_l - 1$, so that

$$V_j = \sum_{l=1}^{4} b_{jl}(\sigma^2_{c,l}) V_l^d. \tag{4}$$

The coefficients $b_{jl}(\sigma_{c,l})$ are calculated from a priori data input into the PRIZMA program which takes into account the results of experiments and computational modeling; the dependence of b_{jl} on $\sigma^2_{c,l}$ is such that $b_{jl}(\sigma^2_{c,l}) \to 0$ as $\sigma^2_{c,l} \to \infty$, and then $W_j \to F_j$, and as $\sigma^2_{c,l} \to 0$ in channels with EDCD, $b_{ll'}(\sigma^2_{c,l}) \to \delta_{ll'}$ ($\delta_{ll'}$ is the Kronecker symbol, and $ll' = 1, 2, \ldots, N_d$), and then $W_l \to W_l^d$. The choice of continuous test functions ψ_{kj} and the use of smooth interpolation of the correction V_j permits producing a microstructure of the recovered distribution which is similar to the microstructure of the calculated energy distribution R_j.

On can judge the objectiveness of the control from the deviations of F_l from W_l^d, in particular, from the quantity

$$\delta^2 = \frac{1}{N_d} \sum_{l=1}^{N_d} |V_l^d|^2 = \frac{1}{N_d} \sum_{l=1}^{N_d} \left| \frac{W_l^d}{F_l} - 1 \right|^2. \tag{5}$$

Upon deterioration of the quality of the a priori information, δ^2 increases, and in accordance with the relationship (1) the role of the local correction V_j, which is dependent on the selected interpolation method, the estimates of the values of $\sigma^2_{c,l}$, and possible individual "spikes" in the EDCD readings, increases. When δ^2 starts to exceed some specified value δ^2_{sp}, it is necessary to introduced new data of the physical computation into the control system.

During the initial period of operation of an RBMK the calculated energy distribution R_j obtained using the BOKR program is in good agreement in the channels having EDCD with the measurement data of W_l^d, which permits maintaining δ^2 at a level $\sim(2\text{-}4) \times 10^{-3}$. However, as the fuel depletion in the active zone increases, the energy distribution in the reactor becomes unstable, which does not correspond to the quasisteady computational model of the reactor. This leads to a significant increase in δ^2 to values $\sim 5 \times 10^{-2}$ and greater, the role of a local correction in the expression (4) increases significantly, and the error in control of the channel power increases.

In practice and in reactor models operating in real time, the energy distribution is stabilized in time intervals significantly less than the characteristic time of development

of time-dependent processes [4]. Therefore, taking account of dynamic effects in the models can be simplified, and as a result it proves to be possible to combine the "usual" two-dimensional quasistatic neutron physics calculation with the optimization calculation.

In order to produce the specified energy distribution or one close to it, the reactor operator with the help of the monitoring and control system performs in essence extremal regulation of the energy distribution in the active zone with a goal function of the type

$$K_r \to \min \tag{6}$$

or

$$\min K_{sf} \to \max, \tag{7}$$

where K_r is the nonuniformity coefficient of the energy distribution over the reactor radius and K_{sf} is the safety factor to the maximally permissible or the specified value of the distribution W_j^{sp}. In practice the goal functions (6) or (7) are realized by maintaining some specified distribution. In this connection it is advisable to take into account the analogous actions of the reactor operator in the calculations with this model in order to reduce unjustified distortions in the calculated macrodistribution obtained with the help of the quasisteady model.

An extremal regulation algorithm is implemented in the program BOKRUS [3], in which the response of the system to displacements of the SCR rods is determined by calculations using the BOKR program. As experience in the operation of RBMK has shown, the energy distributions calculated using the BOKRUS program prove to be close to the actual distributions at very large time intervals. However, one should note that the position of the rods obtained in the calculations may not correspond to those implemented by the operator. Due to this microstructure of the calculated distribution may differ from the microstructure of the energy distribution realized in the reactor, which, as has been noted above, is well predicted by the calculations using the BOKR program with the initial position of the rods. In order to overcome this difficulty, functions calculated in advance of the influence of a shift of the rods on the energy distribution are used. Such corrections to the results of the BOKRUS program are determined from these functions, which bring its microstructure closer to that predicted by the BOKR program without significantly altering the macrodistribution.* The expounded method for preparation of the a priori information permits maintaining the value of δ^2 from the expression (5) within a rather narrow interval which does not exceed 6×10^{-3}. The method has been implemented in a complex of programs which provide for the operation of an RBMK. In order to reduce the computation time, a new algorithm has been developed in which, in contrast to the BOKRUS program, a step-by-step method of regulation of the SCR control rods is used for correction of the iterations in the nuclear fission sources in solving the diffusion equations. Units of the fast BOKR–BIS programs [5] which permit determining immediately after 3-5 internal iterations the direction of variation of the distribution as a function of the insertion depth of the SCR rods, are used to calculate the energy distribution at each iteration. Shifting of the rods is accomplished as follows.

The iteration $Q_j^{(n)}(h^{(m)})$ is calculated for the position of the rods $h^{(m)}$ with a fission source $Q_j^{(n-1)}$ 3-5 internal iterations by the scheme of Buleev and Ginkin [6]). The average powers $\bar{w}_k^{(n-1)}$ and $\bar{W}^{(n)}(h^{(m)})$ in the k-th multicells, which are a set of 3 × 3 cells having a central cell with an SCR rod, are determiend in these iterations. The ordered sequence of numbers

$$\alpha_k^{(n,m)} = \frac{\bar{W}_k^{(n)}(h^{(m)})}{\bar{W}_k^{(n-1)}} - 1, \quad k = 1, 2, \ldots, N_{rod}$$
$$\alpha_1^{(n,m)} < \alpha_2^{(n,m)} < \alpha_3^{(n,m)} < \ldots < \alpha_{N_{rod}}^{(n,m)} \tag{8}$$

*The described method of preparation of the computational data – optimization of the energy distribution by the BOKRUS program and the introduction of corrections to the microstructure – is equivalent to the correction of the breeding properties of multicells with centers in the SCR rods, which leads to a change in the macrodistribution [2].

is constructed, where N_{rod} is the number of rods taking part in the regulation. We choose n^+ and n^- rods, which correspond to the first n^+ and the last n^- terms of the sequence. For these rods commands are issued for extraction to a depth $h_k^{(m+1)} = h_k^{(m)} - \Delta h$, $k = 1, 2, \ldots, n^+$ and for insertion to $h_k^{(m+1)} = h_k^{(m)} + \Delta h$, $k = N_{rod}, N_{rod}-1, \ldots, N_{rod}-n^-$, where Δh is the shift step of the rods (it varies from 0.4 to 0.1 m). One can take $n^+ = n^-$ in the calculations; for best compensation of the reactivity in the regulation process one can alter the relationship between the number of withdrawn and inserted rods, using the estimate k_{ef} of the n-th iteration ($k_{ef} \approx \sum_{j=1}^{N_{HGA}} Q_j^{(n)}(\mathbf{h}^{(m)}) / \sum_{j=1}^{N_{HGA}} Q_j^{(n-1)}$). The number n^+ is specified within the limits from 10 to 20 in the calculations. For each regulation operation the mean square deviation

$$\sigma_{n,m} = \sqrt{\frac{1}{N_{rod}} \sum_{k=1}^{N_{rod}} (\alpha_k^{(n,m)})^2} \qquad (9)$$

is calculated. In the case in which $\sigma_{n,m} < \sigma_{n,m-1}$, regulation is continued with a specified source $Q^{(n-1)}$. When $\sigma_{n,m}$ becomes larger than (or equal to) $\sigma_{n,m-1}$, a replacement of the source occurs: $Q_j^{(n)}(h^{(m)})$ is substituted in place of $Q_j^{(n-1)}$, the reference power distribution $\bar{W}_k^{(n-1)}$ is replaced by $\bar{W}_k^{(n)}$, and the process is repeated with a reduced shift step Δh. The distribution corresponding to the specified energy distribution W_i^{sp}, for which the result of the physical calculation being profiled, is selected as the initial distribution of the fission sources. It is assumed in the BOKR program that the energy distribution W_j follows the distribution of the fission sources:

$$W_j = G_{th} \frac{Q_j}{\sum_{j=1}^{N} Q_j},$$

where G_{th} is the total thermal power of the reactor. Therefore, under these conditions the algorithm under discussion reduces the discrepancy between successive external iterations, which is equivalent to an acceleration of the iterative process. The algorithm permits reacting to incipient distortions of the energy distribution caused by the effect of interference of the rods shifted, and with a small shift step one can achieve the maximum approach of the result of the iterative process to the specified energy distribution (according to the criterion of the average power of the channels surrounding each rod).

The computational results show that for the RBMK computational model the contribution to optimization of the regulation in the first 4-6 external iterations, when the solution acquires practically all the regularities of the computational model, is the most important. The results of the optimization depend little on whether or not the external iterations which remained are performed with regulation or without it.

The algorithm discussed has been implemented in the program OPTIMA written in the FORTRAN-4 language for series ES computers. The computation time of one version of the program is about 20 min of machine time on an ES-1033 computer. The input of initial data from punched tape output from the "Skala" CCS is implemented in the program, and output of the computational results onto punched tape in the form required for input into the control system is also provided for. The OPTIMA program has been subjected for an extended time to experimental checking by means of calculations of specific states of an RBMK-1000 for the first and second units of the Kurskaya and Chernobyl'skaya nuclear power plants. The possibility of the application of the results obtained to the control system was checked with the help of calculations using the PRIZMA program (see Table 1). It is evident that the OPTIMA program significantly improves the quality of the physical calculation in comparision with the usual calculations by the BOKR program. When the results are used for control of the channel power in channels with EDCD, the deviations between the objective estimate of the energy distribution F_ζ and the measured power W_ζ are reduced. A comparison is made for the following parameters: K_r; G_{th}, recovered by the PRIZMA program (or by the PRIZMA—ANALOG program, which simulates on a computer the operation of the plant PRIZMA program); W^{max}; the minimum safety factor until a heat exchange crisis K_{sf}^{min}; the thermal engineering reliability of the reactor H; and the dispersion of the energy distribu-

TABLE 1. Computational Results Using the OPTIMA Program

Nuclear power plant unit	Date	K_r		σ_2, $(\%)^2$	σ^+_{max}, %	σ^-_{max}, %	σ^d_2, $(\%)^2$	Plant PRIZMA		
		BOKR	OPTIMA					K_r	G_{th}, MW	W^{max}_j, MW
Kurskaya I	06.03.79	1,602	1,346	6,7	17,6	13,9	6,2	1,306	3115	2,52
II	27.03.80	1,604	1,279	4,5	20,8	14,3	4,8	1,276	3202	2,66
Chernobyl'skaya I	19.01.81	1,812	1,432	6,2	13,4	18,1	5,8	1,430	3179	2,75
II	23.01.81	1,738	1,404	5,3	11,2	17,4	4,6	1,382	3226	2,69

Nuclear power plant unit	Plant PRIZMA			PRIZMA–ANALOG with calc. by OPTIMA program					
	K^{min}_{sf}	D_n	H	K_r	G_{th}, MW	W^{max}_j, MW	K^{min}_{sf}	D_n	H
Kurskaya I	1,12	18,8	0,998367	1,306	3117	2,50	1,12	13,0	0,998378
II	1,04	55,0	0,996050	1,277	3198	2,65	1,04	28,2	0,996337
Chernobyl'skaya I	1,09	72,0	0,998279	1,430	3174	2,73	1,09	53,8	0,998288
II	1,14	39,0	0,998279	1,380	3221	2,70	1,14	25,0	0,998294

tion $D_n = \delta^2 - \frac{1}{N_d}\sum_{l=1}^{N_d}\sigma^2_{c,l}$. The energy distribution obtained at nuclear power plants by the PRIZMA program with use of the data of the physical calculation by the BOKRUS program was used in the calculations as the specified W^{sp}_j. The mean-square deviations σ_2 of the results of calculating the power W^{opt}_j by the OPTIMA program and the data of the plant PRIZMA program are indicated in Table 1, along with the maximum relative excess $\sigma^+_{max} = \max_j (W^{opt}_j / W^{sp}_j - 1)$ and understatement $\sigma^-_{max} = \max_j (1 - W^{opt}_j/W^{sp}_j)$, and the mean-square deviation σ^d_2 calculated for the channels with EDCD.

The results of calculations using the OPTIMA program show that one can achieve and appreciable reduction of K_r in comparison with the results of the physical calculation using the BOKR program in the regulation of the insertion depth of the SCR rods. The introduction of such an energy distribution in the "Skala" CCS permits improving the values of D_n and maintaining the remaining parameters practically constant. OPTIMA is a newfast program which provides for equalization of the energy distribution in an RBMK by means of changing the insertion depth of the SCR rods, and it is completely suitable for use in the complex of programs which provide for operation of an RBMK.

In order to increase the informativeness of the estimate of the mathematical expectation of the energy distribution for reactors with an unstable distribution, it is necessary not only to detail the model of the reactor and to refine the description of the dynamic effects in it, but also to introduce, mainly into the physical calculation, a unit for the automatic optimization of the distribution with the goal control function adopted for a given reactor.

LITERATURE CITED

1. N. A. Dollezhal' and I. Ya. Emel'yanov, A Channel Power Reactor [in Russian], Atomizdat, Moscow (1980).
2. A. A. Shkurpelov, N. V. Isaev, and A. S. Nemirov, At. Energ., 50, No. 1, 6 (1981).
3. I. Ya. Emel'yanov, V. V. Postnikov, and G. V. Yurkin, At. Energ., 47, No. 1, 8 (1979).
4. E. V. Filipchuk, P. T. Potapenko, and V. V. Postnikov, Control of the Neutron Field of a Nuclear Reactor [in Russian], Énergoizdat, Moscow (1981).
5. A. A. Shkurpelov et al., At. Energ., 50, No. 5, 352 (1981).
6. G. I. Marchuk, Methods of Numerical Mathematics, Springer-Verlag (1975).

CONTROL OF THE NEUTRON DISTRIBUTION IN A REACTOR

V. N. Konev
and B. Z. Torlin

UDC 621.316

The stability of the neutron distribution in a reactor having special systems of local automatic control (LAC) has been studied in a number of papers [1-3]. As a rule, the systems considered had a small number of control rods (CR), and to each LAC was conventionally assigned the part of the core controlled by it with intrareactor control sensors and/or external chambers, producing jointly a control signal for "its own" rod located in this same region of the reactor. In determining the stability of such systems certain characteristic computational difficulties sometimes arose if the regions controlled by the various LAC were not clearly delimited. Such difficulties arose in the analysis of the stability of the optimum solution when many CR were used [4-6].

The influence functions of the CR play an important role in control problems. We use the definition of the influence function ψ_j of the j-th CR given in [7]. We call the value of this function in the zone of the i-th sensor the influence coefficient ψ_{ij} of the j-th CR on the i-th sensor. If ρ_i is a sufficiently small change of the effectiveness of the j-th CR, its influence on the i-th sensor is $\psi_{ij}\rho_i$. Let χ_i be the change in response of the i-th sensor as the result of a small perturbation of the properties of the reactor not related to the change in effectiveness of its CR, and φ_i the change in response of the i-th sensor as a result of the simultaneous action of these effects. Then*

$$\varphi_i = \sum_{j=1}^{N} \psi_{ij}\rho_j + \chi_i; \quad i = 1, 2, \ldots M, \tag{1a}$$

where N is the number of CR and M is the number of sensors. In matrix form

$$\boldsymbol{\varphi} = \hat{\Psi}\boldsymbol{\rho} + \boldsymbol{\chi}. \tag{1b}$$

Of the possible algorithms for the control† of the neutron distribution, the simplest is

$$\boldsymbol{\varphi} = 0 \quad \text{for} \quad M = N. \tag{2}$$

In practice, if each sensor is located close enough to "its own" CR, and there are the same number of CR and sensors, the matrix‡ $\hat{\Psi}$ will be diagonally dominant and well-conditioned. It was shown in [3] that if the sensors are too near the rods, the neutron distribution becomes unstable.

Let us consider the neutron distribution stabilization system discussed in [3], which employs six symmetrically placed chambers and six CR located along the radial lines drawn from the center of the reactor to the chambers. When the CR are located near the chambers, the system has a very low stabilizing capability. As the CR are moved away from the chambers,

*For simplicity we assume that the reactor has a fast power reactivity effect (see note in [7].

†From now on we assume that the control system is sufficiently quick-acting in the sense indicated in [8, 9].

‡ In this case the influence matrix $\hat{\Psi}$ is not only square, but also plays the role of the control matrix.

Translated from Atomnaya Énergiya, Vol. 54, No. 6, pp. 390-395, June, 1983. Original article submitted July 8, 1982.

 0038-531X/83/5406-0394$07.50

the stabilization is improved, but when the CR are near the center of the reactor, all the elements of the matrix $\hat{\psi}$ approach the same value, and the condition of $\hat{\Psi}$ is sharply worsened. If the CR are located at the same radius on the bisectors of the angle formed by the lines drawn from the center to the chambers, the matrix $\hat{\Psi}$ becomes singular — its determinant is zero. This is true for the CR at any radius, and for any even N = M.

The operating algorithm for the LAC system of the RBMK reactor at the Leningrad nuclear power plant [10, 11] is rather simple, but more complicated than the system discussed above:

$$\varphi_r = 0, \tag{3}$$

where the components of φ_r are the total signal $\sum_{k=1}^{4} \varphi_{i_k}$ of the deviation of the responses of four snesors surrounding the i-th rod of the LAC. The elements of the control matrix are $\sum_{k=1}^{4} \psi_{i_k j}$. Obviously, as long as the limits of the region controlled by the sensors of each CR are clearly enough delineated, the control matrix will be diagonally dominant and well-conditioned. In the case under consideration there are many more sensors than CR in the automatic control system, and therefore there are many possible ways of using this redundancy. For example, the stability of control systems with least-square deviation (LSD) from the specified neutron distribution was investigated in [3, 7, 12]. It was shown in [7] that when there is a fast power reactivity effect the control algorithm has the form

$$\hat{\Psi}^{\mathrm{T}} \varphi = 0, \tag{4}$$

where T denotes the transpose.

The control signal for the CR is now formed by all the sensors in the system, and not just by the nearest one. Therefore, there are no "own" and "other" sensors. The control matrix is formed by substituting Eq. (1) into (4) in the form $\hat{\Psi}^{\mathrm{T}}\hat{\Psi}$. In general it is difficult to draw a conclusion about its condition. It can be shown that such a control matrix will be strongly diagonally dominant if the CR and sensors form a regular lattice and there are many more sensors than CR.

In the RBMK there are more CR than sensors in the radial power distribution control system [10, 11]. Therefore, e.g., including all the CR and sensors in the automatic control system raises the problem of the redundant CR, which can be solved in various ways, in particular, by the principle of least action of the rods $\min_{\rho_j} D = \sum_{j=1}^{N} \rho_j^2$. In this case the operating algorithm of the control system has the form

$$\varphi = 0; \tag{5a}$$

$$\rho + \hat{\Psi}^{\mathrm{T}}\lambda = 0. \tag{5b}$$

The components of the M-dimensional vector λ are Lagrange multipliers which have a clear physical meaning. This is easy to understand after substituting Eq. (1b) into (5a), and then (5b) into the result. The control matrix takes the form $\hat{\Psi}\hat{\Psi}^{\mathrm{T}}$. Control is accomplished, as it were, by group motions of the CR, and the λ_i play the role of the effective displacement of the group. According to Eq. (5b), the displacements of the CR in the group must be proportional to their influence coefficients. By replacing the CR by sensors and the sensors by CR and using the reciprocity property [13], it is easy to establish the "conjugacy" of the control by the principle of least action with LDS. Therefore, the above statement about the condition of the control matrix remains valid.

We have considered the simplest neutron distribution control algorithms based directly on sensor responses. Optimal control algorithms are more sophisticated. For control by slow processes using a system of quick-acting controls, the optimal solution can be obtained by linear programming methods [5, 6]. In this case the number of operative CR determines the number of channels reaching their maximum restricted temperature. We call these hot channels. For sufficiently small perturbations the optimal process will preserve the hot-channel parameters, i.e., it will follow algorithm (2). Now φ combines the power deviations of the hot channels and not the sensor responses. This may have an unfavorable effect on the

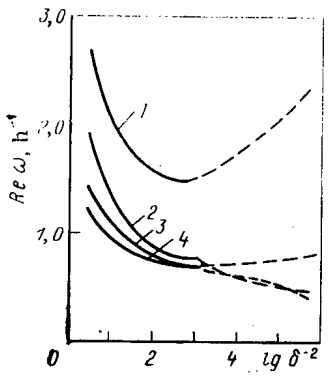

Fig. 1. Dependence of Re ω on δ^{-2}: 1, 2) for Figs. 2c, 2a; 3, 4) for Figs. 2f, 2e; dashed curve indicates the region of poor numerical stability.

condition of the matrix $\hat{\Psi}$ for the influence of the CR on the hot channels. This is related to the fact that in contrast with sensors, whose disposition can be planned beforehand, the location of the channels is determined after solving the optimization problem, and may turn out to be anywhere. Some of the variations of the location of hot channels may be unfortunate from the point of view of the condition of the matrix $\hat{\Psi}$. Let us analyze the conditions of its degeneracy. Suppose N hot channels are located in such a way that one of the rows ψ_i of the matrix $\hat{\psi}$ is a linear combination of the others. We number the hot channels in such a way that this row and the channel associated with it have the number N, i.e.,

$$\sum_{i=1}^{N-1} \psi_i^T l_i = \psi_N^T. \tag{6}$$

Considering ψ_N^T as a function of the displacement of the N-th channel, we can obtain the equation of the singular line, motion along which will leave the matrix $\hat{\psi}$ degenerate:

$$\sum_{i=1}^{N-1} \psi_i^T dl_i = \frac{\partial \psi_N^T}{\partial x} dx + \frac{\partial \psi_N^T}{\partial y} dy. \tag{7}$$

Obviously, the line or lines can pass through any of the remaining hot channels. Thus, when x and y coincide with the coordinates of the k-th hot channel, at least N − 1 choices of initial conditions of the form $l_i = \delta_{ik}$ and $\psi_N^T = \psi_k^T$ for any $k < N$, where δ_{ik} is the Kronecker symbol, are determined for system (7). With these initial conditions the singular lines passing through all the hot channels from the first to the (N−1)-th can be determined* from system (7). If the control matrix is well-conditioned, the N-th hot channel must not turn out to be too close to one of these lines. Since it is impossible to guarantee that this condition will be satisfied, we examine the dangers accompanying its violation and how to avoid them. If the control matrix is ill-conditioned (in the present case this is the error in the determination of ρ, the displacement of the CR, by algorithm (2) $\hat{\Psi}\rho + \chi = 0$), gross errors will appear in the solution, even at a low noise level, e.g., in the responses of the sensors or in the determination of the power distribution deviation vector in hot channels. This is a typical case of low noise stability, when a small random error in measurement is transformed into large-scale random fluctuations of the whole state vector of the system, or part of it. In the present case the conditions $\varphi = 0$ can be satisfied rather accurately

*Because of the Binet–Cauchy formula [14], the control matrix $\hat{\psi}^T\hat{\psi}$ with LSD for M > N may become singular if all (!) M sensors turn out to be on the intersections of the singular lines of all combinations of them N − 1 at a time. If there are considerably more sensors than rods, this is extremely improbable. By the principle of least action, the same considerations for the control matrix $\hat{\psi}\hat{\psi}^T$ are valid for M < N.

and ρ undergoes appreciable random fluctuations. If the matrix $\hat{\Psi}$ were singular,* this condition could not be satisfied exactly for any displacements ρ, and it would have to be satisfied approximately. It is advisable to do this even when $\hat{\Psi}$ is ill-conditioned, since it improves the correctness of the control problem considerably.

If the concept of admissible straggling parameters δ_φ and δ_ρ is introduced, the control algorithm based on a combination of minimization of the deviation of the power distribution in hot channels and the action of the CR

$$\min_{\rho_j}\left(\sum_i \frac{\varphi_i^2}{\delta_\varphi^2}+\sum_j \frac{\rho_j^2}{\delta_\rho^2}\right)$$

will have the form

$$\sum_i \psi_{ij}\varphi_j+\delta^2\rho_j=0 \text{ for } j=1, 2, \ldots, N, \tag{8a}$$

where

$$\delta^2=(\delta_\varphi/\delta_\rho)^2$$

or in matrix form

$$\hat{\Psi}^\varphi\varphi+\delta^2\rho=0. \tag{8b}$$

After substituting Eq. (1b) into (8b), we obtain the control matrix in the form $\hat{\Psi}^T\hat{\Psi}+\delta^2 E$, where E is the unit matrix. Now the control matrix is positive definite, and its condition may be affected by δ, a single regularizing parameter determined solely by the ratio $\delta_\varphi/\delta_\rho$. The control matrix was found to be ill-conditioned in studies with the BASIRA program of the stability of the solution close to that derived in [6] for two-dimensional power distribution. The spacings of the hot channels and CR were taken from [6] and transferred approximately to the RBMK loading diagram. Feedbacks and the reactivity coefficients characteristic of this reactor with 1.8% enriched fuel were used.† In the absence of a spatial stabilization system, the unstable mode with the shortest period for a single automatic control — the first azimuthal — develops in $\tau_{01}\approx 2$ min.

The incorrectness of the problem before the introduction of regularization appears in the form of instability of the calculation of the principal eigenvalue.‡ In these cases the spectral condition number [17] of the control matrix (the measured ratio of its maximum and minimum singular numbers [18]) turned out to be greater than 10^4. This kind of trouble never arose if the CR and sensors, e.g., formed a regular lattice and were near one another. In using the control algorithm in the form (8), the principal eigenvalue can be determined reliably without fear of a numerical instability of the solution. However, the inroduction of δ into the control algorithm worsened the dynamical stability of the

*The simplex method [15] for solving the linear programing problem and modifications of it cannot lead to a singular matrix $\hat{\Psi}$, but it cannot guarantee that the control matrix will be well-conditioned. This appears, e.g., in a weak sensitivity of the optimum coefficient of nonuniformity of the power distribution to different variations of ρ_{opt} obtained with different versions of the programs.

†The power reactivity coefficient is 0.005, the temperature reactivity coefficient of graphite is 0.013 with a time constant of 1 h, and the xenon reactivity coefficient is 0.0298 [16].

‡To analyze the stability the BASIRA program determines the eigenvalue ω of the system of transient equations with the maximum real part [16].

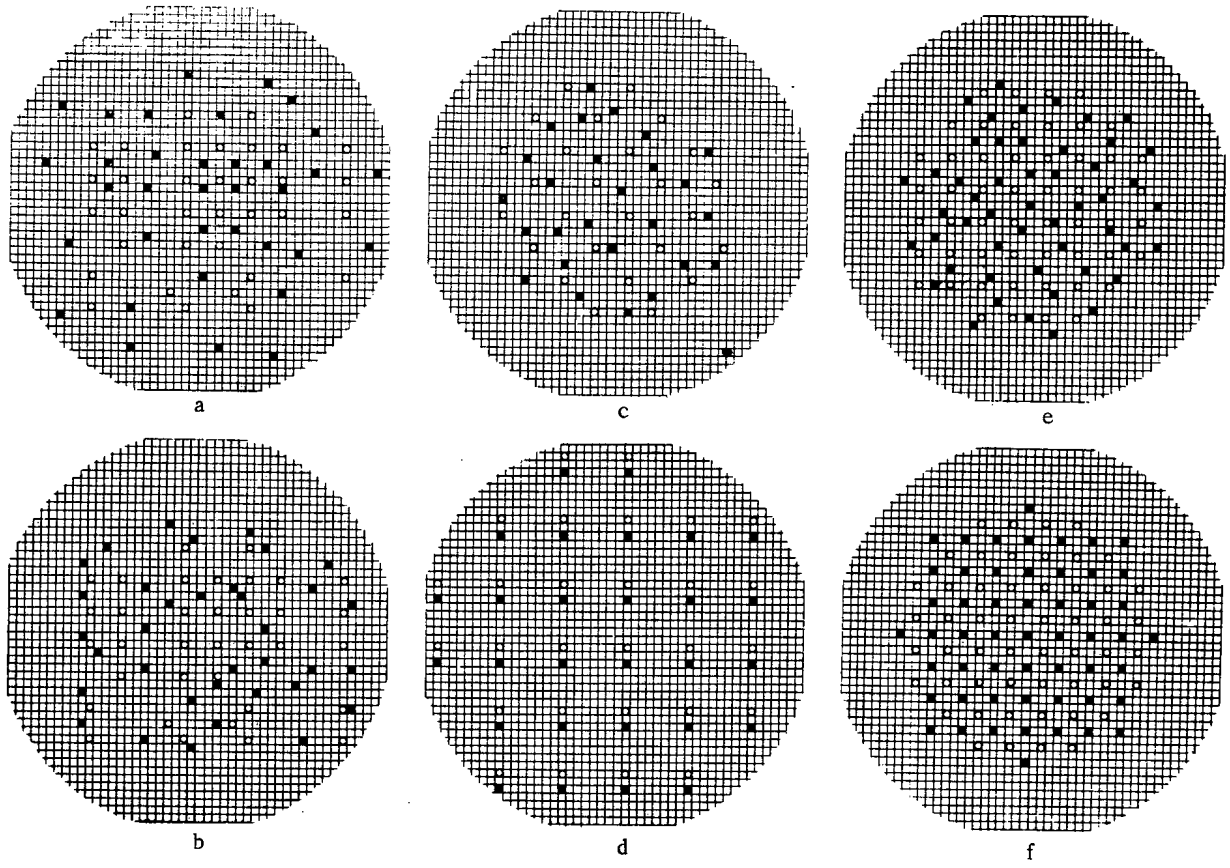

Fig. 2. a, b, c, d, e, f: ■) hot channels; ○) CR.

reactor. This change of the control algorithm is equivalent to a change from an astatic to a static control law with a large amplification factor ($\sim\delta^{-2}$). For a reliable guarantee of the numerical stability of the problem it is sufficient to have $\delta^2 \approx 10^{-4}$ of the maximum eigenvalue of the control matrix. Of course, this does not affect the stability of a system whose control matrix is well-conditioned. However, δ has an apprecialbe effect on the stability of systems with ill-conditioned control matrices. Figure 1 shows the dependence on δ of the real of the principal eigenvalue ω of systems with CR and hot channels in the positions shown in Figs. 2a, b, e, and f. As $\delta \to 0$ it should be possible to determine the asymptotic value of Re ω corresponding to an astatic control law. Unfortunately, in a number of cases, as in the present situation when the spectral condition number becomes larger than 10^4, this fails because of numerical instability.* Therefore, in subsequent calculations we chose a single value $\delta^2 = 2.5 \times 10^{-4}$. The straggling δ_ρ, which is one-third the travel of a RBMK-1000 control rod, corresponded to $\delta_\varphi \sim 0.5$ % in the value of φ/Φ_0.

A study of systems with CR and hot channels in various positions showed that stability is determined largely by how extensively the whole core is covered by control. Figure 2 shows the positions of RBMK-1000 CR and hot channels for some of the larger number of cases calculated. The arrangement of CR and 35 hot channels shown in Fig. 2b is similar to that in [6]. Figure 2a differs from Fig. 2b only in the positions of hot channels, which are now more widely spaced in the core. Figure 2c differs from Fig. 2b primarily in having only 26 CR and hot channels, but arranged so that the region they control is not too different from the analogous region in Fig. 2b. Finally, Fig. 2d shows the locations of 28 CR arranged in a regular lattice covering the whole core. The sensors are also spaced reguarly at distances of two lattice constants from the CR. Figures 2e, f show the positions of 52 CR and hot channels covering practically the whole controlled region of the reactor. In this case all the rods of the plateau region take part in control, and therefore they form a regular lattice. Figure 2e differs from Fig. 2f in using regularly spaced radial control sensors.

*The spectral analysis of the control matrices was performed with the KIM and QREIG programs from the library of standard BÉSM-6 programs 18]. A test showed that the calculated small eigenvalues ($< 10^{-4}$) of ill-conditioned matrices have large, even-order-of-magnitude, errors.

The characteristic times for the development of instability are 1.45, 0.61, and 0.58 h for Figs. 2a, b, and c respectively. These values show how much a broad coverage of the core by control contributes to the improvement of stability, especially for Fig. 2d for which the system turned out to be stable even for close spacing of the sensors around the CR. Separation of the sensors or hot channels from the CR improves the stability considerably. Systems corresponding to Figs. 2e, f turned out to be unstable, in spite of the large number of CR. This can be accounted for by the fact that here the whole peripheral region, whose area is half that of the core, remained without control. The characteristic times of development of instability for Figs. 2e, f are 1.37 and 1.53 h, respectively. The irregularity in the location of the hot channels had little effect on the instability characteristics.

In conclusion, we point out another possible control variant. If the matrix $\hat{\Psi}$ and the related matrix $\hat{\Psi}^T\hat{\Psi}$ are ill-conditioned, there are very small eigenvalues in the $\hat{\Psi}^T\hat{\Psi}$ spectrum. The proper motions of CR, ρ_ν, corresponding to these small eigenvalues are practically useless for correcting the deviation vector φ. Hence, there is one other method of regularization of the control problem. Taking account of the LSD principle for the condition $(\rho, \rho_\nu) = 0$, we obtain the control algorithm in the form

$$\begin{aligned} \hat{\Psi}^T\varphi + \sum_\nu \lambda_\nu \rho_\nu = 0; \\ (\rho, \rho_\nu) = 0, \end{aligned} \tag{9}$$

where the λ_ν are Lagrange multipliers. Eigenvalues which are 10^{-4} of the largest value or smaller must be called "very small". Algorithm (9) also has good numerical stability. Calculation performed with it and with algorithm (8) gave nearly the same results.

The authors thank A. A. Anikin, A. M. Afanas'ev, A. D. Galanin, B. P. Kochurov, Ya. V. Shevelev, and others for a discussion of the work and a number of valuable comments.

LITERATURE CITED

1. V. I. Budnikov et al., At. Energ., 45, 331 (1978).
2. I. Ya. Emel'yanov, At. Energ., 47, 370 (1979).
3. B. Z. Torlin, At. Energ., 48, 297 (1980).
4. I. Ya. Emel'yanov, V. V. Postnikov, and G. V. Yurkin, At. Energ., 47, 8 (1979).
5. I. Ya. Emel'yanov, V. G. Nazaryan, and V. V. Postnikov, At. Energ., 44, 310 (1978).
6. A. A. Anikin and Ya. V. Shevelev, Problems of Atomic Science and Engineering. Series Dynamics of Nuclear Power Installations [in Russian], No. 3, p. 35 (1980).
7. B. Z. Torlin, At. Energ., 47, 415 (1979).
8. A. M. Afanas'ev and B. Z. Torlin, At. Energ., 49, 323 (1980).
9. B. Z. Torlin, At. Energ., 49, 324 (1980).
10. N. A. Dollezhal' and I. Ya. Emel'yanov, Channel Nuclear Power Reactors [in Russian], Atomizdat, Moscow (1980).
11. I. Ya. Emel'yanov et al., At. Energ., 49, 357 (1980).
12. A. M. Afanas'ev and B. Z. Torlin, At. Energ., 48, 121 (1980).
13. B. Z. Torlin, At. Energ., 46, 189 (1979).
14. F. R. Gantmakher, The Theory of Matrices, Chelsea, New York (1959).
15. S. I. Zukhovitskii and L. I. Abdeeva, Linear and Convex Programming [in Russian], Nauka, Moscow (1967).
16. V. N. Konev and B. Z. Torlin, At. Energ., 53, 25 (1982).
17. J. K. Wilkinson, The Algebraic Eigenvalue Problem, Clarendon, Oxford (1965).
18. V. V. Voevodin, Linear Algebra [in Russian], Nauka, Moscow (1974).
19. G. L. Maznyi, Programming the BÉSM-6 in the "Dubna" System [in Russian], Nauka, Moscow (1978).

CALCULATION OF CRITICAL HEAT FLUX IN ROD BUNDLES WITH LOCAL TURBULATORS

V. K. Ivanov
and L. L. Kobzar'

UDC 536.242

Reserve before a heat-transfer crisis in boiling of coolant is an important index of the reliability and safety of a nuclear reactor. One way of increasing this index is to place special devices in the flow core to modify the coolant flow. This method of increasing the critical heat loads has been studied at the I. V. Kurchatov Institute of Atomic Energy (IAE) [1, 2]. The spacing lattice-intensifiers for RBMK-1500 fuel-element assemblies were chosen on the basis of experimental data and the results of research performed at other organizations.

Earlier [2] a procedure was developed for calculating the hydraulic resistance coefficient of heat-transfer intensifiers based on their geometrical characteristics. The hydraulic resistance coefficient of a lattice-intensifier is given by the expression

$$\zeta = C(\Phi/F_0)^2, \tag{1}$$

where $C = 7.145$ is an empirical constant, and F_0 is the total straight-through cross section of the channel;

$$\Phi = \int_F f(\gamma)\, dF; \tag{2}$$

F is the area of the elements of the lattice in plan (midsection); $f(\gamma)$ is a fucntion of the angle of inclination of an elementary area to the direction of free-stream flow (angle of attack);

$$f(\gamma) = \begin{cases} \sin^2 2\gamma & \text{for } 0 \leqslant \gamma < \pi/4; \\ 1 & \text{for } \pi/4 \leqslant \gamma \leqslant \pi/2. \end{cases} \tag{3}$$

The proposed procedure is in good agreement with experimental data. The maximum error of the calculation is 6%.

After solving the problem of the hydraulic resistance of the intensifiers, it was possible to proceed to the next problem — the calculation of the increase in the critical heat loads as a result of using lattice-intensifiers.

A number of procedures for calculating critical heat fluxes in rod bundles have been developed in the USSR and abroad. One of these procedures originated in the I. V. Kurchatov IAE [3]. It is in good agreement with experiment, but like other similar procedures based on experimental data on bundles with ordinary spacing lattices, it cannot be applied to heat-transfer intensifiers. According to the IAE procedure, the critical heat flux in the running longitudinal coordinate z for rod bundles with ordinary spacing lattices and a uniform distribution of heat release is given by the formula

$$Q = \left(D - \frac{X}{3.5}\right) \frac{1}{345\,(1 + z/l)}, \tag{4}$$

Translated from Atomnaya Énergiya, Vol. 54, No. 6, pp. 395-399, June, 1983. Original article submitted May 10, 1982.

 0038-531X/83/5406-0400$07.50

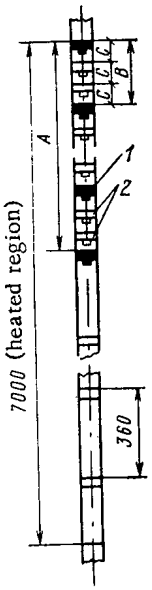

Fig. 1. Schematic diagram of placement of lattice-intensifiers along height of models: lattice-intensifiers spacing all rods of model (lattice of the first kind) (1); six rods of model (lattice of the second kind) (2); 3) regular RBMK-1000 spacing lattice with a 360-mm tice constant.

TABLE 1. Types of Lattice-Intensifiers and Their Positions along the Height of a Fuel-Element Assembly for Various Models (Fig. 1)

Model	Type of lattice intensifier [2]	A, mm	B, mm	C, mm
I	1	4290	206	—
II	2	3960	360	120
III	3	4320	360	120
IV	4	4320	180	—
V	5	3600	180	—
VI	3	3600	360	180
VII	3	3600	240	—

where Q and X are generalized expressions for the critical heat flux q_{cr} and the relative enthalpy x of the coolant; $\ell = 3.54$ m. For D = 0.942, Eq. (4) describes the experimental data obtained on models with regular RBMK-1000 spacing lattices in the pressure range (7.35 ± 0.5) MPa with a mean square error of 4%.

The approach to the calculation of critical loads in bundles with lattice-intensifiers developed in the present article is based on the IAE procedure. The IAE formula is used in a form expressing q_{cr} as a function of the underheating Δi_{in} of the coolant before saturation at the channel entrance. This form of the formula is obtained by substituting the heat-balance equation into Eq. (4).

The results of experiments performed on the KS stand on critical heat loads and hydraulic characteristics of full-scale models of RBMK-1500 fuel-element assemblies, and the geometrical characteristics of the models and lattice-intensifiers, were given in [1, 2] (Table 1).

There is no published information on such methods of calculating critical heat loads in rod bundles with heat-transfer intensifiers which takes account of the geometrical features of the intensifiers and their spacing. Available correlations for calculating critical loads are based on the results of experiments with ordinary spacing lattices. Of course, any spacing lattice is also an intensifier. However, it is very difficult to establish the effect of the structure of such lattices on the conditions of approach to a heat-transfer crisis from experimental data, since the effect is small. This is accounted for, first of all, by the fact that spacing lattice structures are generally chosen to minimize their effect on coolant flow, and secondly, that the distance between spacing lattices is generally chosen to be rather large, and their effect decreases along the flow path from one lattice to another.

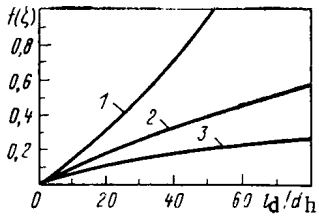

Fig. 2. Plots of Eq. (7) for: 1) B = 20; 2) 30; 3) 40.

An attempt was made in [4] to take account of the intensifying effect of spacing lattices by using the following relation to estimate the ratio of the critical heat flux in a rod bundle with spacing lattices to that in an ideal bundle (without spacing lattices):

$$q_{cr}^{int}/q_{cr}^{id} = 1 + 0.3\ \exp(-l_d/40d_h), \tag{5}$$

where l_d is the distance between lattices, and d_h is the hydraulic diameter.

Smolin and Polyakov [4] obtained a rather simple expression, although they processed a large mass of test data for various experimental ranges. They found no dependence on the type of spacing lattices, probably because in most of the experimental ranges for which they processed data the lattices used were of nearly the same construction and had nearly the same effect on the flow. In addition, the attempt to establish a difference in the effects of various types of lattices apparently failed because this difference is small. Relations similar to (5) cannot be used to estimate the increase in critical loads in bundles with effective intensifiers, since such relations do not reflect the structural peculiarities of the intensifiers, and do not adequately take account of the character of the distribution of intensifiers along the length of the bundle.

In the procedure described below, all the geometrical characteristics of the rod bundle are taken into account. The procedure is based on the following assumptions:

The effect of the basic system parameters (pressure, mass velocity, vapor content) on the conditions of approach to a heat-transfer crisis for rod boundles with lattice-intensifiers is assumed to be qualitatively the same as for bundles with ordinary spacing lattices. This assumption permits the determination of critical loads in bundles with lattice-intensifiers by using the correlation of rod bundles with ordinary spacing lattices and corrections to it which take account of the characteristics of the lattice-intensifiers and how they are arranged.

We consider lattices with a rather uniform distribution of intensifying elements over the cross section of a rod bundle. This assumption enables us to stay within the framework of a one-dimensional calculation.

We assume that the main part of the elements of the lattice-intensifiers is concentrated in the flow core and not at the heat-transfer surface.

A dispersion-annular flow regime is assumed.

No distinction is made in the character of the action of the elements of the lattice-intensifiers on the flow (turbulization, deflection, mixing, twist, etc.). It is assumed that in the last analysis these effects lead to turbulation of the flow, and contribute to better mixing. Improved mixing of the coolant helps produce more intense washing of the heat-transfter surfaces by moisture from the core flow.

The intensifying effect is determined by the hydraulic resistance coefficient of the lattice, and falls off exponentially with the distance downstream from the lattice. The intensifying effects of lattices placed one after another are summed.

By using these assumptions the increase in the critical load resulting from the use of intensifiers can be described by the expression

$$q_{cr}^{int}/q_{cr}^{id} = 1 + \sum_{n=1}^{N} f(\zeta_n) \exp\left(-\frac{1}{B}\frac{z-z_n}{d_h}\right), \tag{6}$$

where $f(\zeta_n)$ is the local effectiveness of the n-th intensifier, N is the number of intensifiers before the cross section with coordinate z, and B is an empirical constant.

A comparison of Eqs. (5) and (6) shows the difference of the approaches in [4] and in the present article, but this should not lead to a difference in the final results. As applied to the present case, this amounts to requiring that the increase in the critical load in "weak" parts of a bundle – before the lattices – be the same whether calculated by Eqs. (5) or (6).

Having considered the case of a uniform distribution of identical intensifiers, and having used on the right-hand side of (6) an expression for the sum of terms of an infinitely decreasing geometric progression, we can derive from Eqs. (5) and (6) a relation which gives some reference points in the determination of the values of B and $F(\zeta)$:

$$f(\zeta)=0.3\ \exp\left(-\frac{1}{40}\frac{l_d}{d_h}\right)\Big/\left\{\exp\left(-\frac{1}{B}\frac{l_d}{d_h}\right)\Big/\left[1-\exp\left(-\frac{1}{B}\frac{l_d}{d_h}\right)\right]\right\}. \qquad (7)$$

Figure 2 shows plots of Eq. (7) with B as a parameter; $f(\zeta)$, which according to the logic of the preceding discussions should by a constant, turned out to depend strongly on the lattice pitch. It is more convenient to return to a discussion of Fig. 2 somewhat later.

The results obtained on the KS stand were processed in accordance with Eq. (6). The ratios of the critical heat fluxes for models with lattice-intensifiers q_{cr}^{int} to the critical heat fluxes for a model with regular RBMK-1000 lattices $q_{cr}^{r.l.}$ were determined. The calculated ratios were presented as a function of the mass velocity of the coolant ρw for constant values of the pressure p and the water temperature t_{in} at the channel entrance. Analysis of these results showed that the increase in critical power as a result of the intensifiers was insensitive to a change of system parameters. Consequently, the effect of an increase of the critical load as a result of using a specific type of intensifier can be described by a constant independent of the system parameters.

It should be emphasized that the values of the effectiveness of lattice-intensifiers and a regular RBMK-1000 lattice are compared for identical values of the coolant temperature at the channel entrance. This condition must be satisfied in the future in comparing values of critical loads for various models. This necessitates using Eq. (4) in a form expressing q_{cr} as a fucntion of Δi_{in} in determining critical loads for a model with regular RBMK-1000 lattices. In future references it will be assumed that Eq. (4) is written in such a form.

Table 2 lists the average values of the ratio $q_{cr}^{int}/q_{cr}^{r.l.}$ for all models investigated with lattice-intensifiers.

It is convenient to write the critical heat flux for a bundle with lattice-intensifiers in the form

$$q_{cr}^{int}=\frac{q_{cr}^{int}/q_{cr}^{id}}{q_{r.l.p}/q_{cr}^{id}}\,q_{cr}^{r.l.}. \qquad (8)$$

The values of q_{cr}^{int}/q_{cr}^{id} and $q_{cr}^{r.l.}/q_{cr}^{id}$ are calculated from Eq. (6), and $q_{cr}^{r.l.}$ from (4) with D = 0.942.

The selection of the form of the function $f(\zeta)$ in Eq. (6) was based on the following arguments. The effect of an increase of the critical power must increase with an increase in the hydraulic resistance of a turbulator, but not without limit. For certain values of ζ the effectiveness of a turbulator must increase less rapidly and reach some limiting values. Such a variation of the local effectiveness of a turbulator with increasing ζ can be described by the expression

$$f(\zeta)=A\{1-\exp[(-\zeta/m)^n]\}, \qquad (9)$$

where A characterizes the maximum effectiveness of the turbulator.

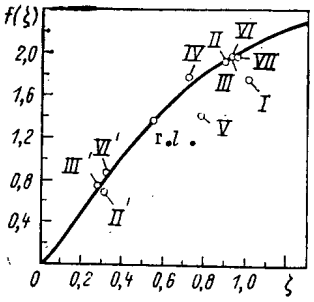

Fig. 3. Dependence of local effectiveness of lattice-intensifiers on the hydraulic resistance coefficient: r.l.) regular lattice of RBMK-1000; ———) calculated from Eq. (9).

We list below the values of ζ for all the lattices used in the experiments. The calculated values are negligibly different from the experimental data in [2]:

Regular RBMK-1000 lattice	0.56
Lattice 1	1.015
Lattice 2	
first form	0.893
second form	0.318
Lattice 3	
first form	0.92
second form	
for models III and VII	0.285
for model VI	0.33
Lattice 4	0.72
Lattice 5	0.77

Based on the processing of the experimental data in accordance with Eqs. (8), (6), and (9), B = 20, A = 2.54, m = 0.7, and n = 1.3.

The average values of $q_{cr}^{int}/q_{cr}^{r.l}$ computed with these values of the empirical constants, and the errors of the calculation, are listed in Table 2. For the regular RBMK-1000 lattice, $f(\zeta) = 1.32$ and $q_{cr}^{r.l}/q_{cr}^{id} = 1.18$. The mean-square error of the calculation for the whole mass of experimental points is 6.7%.

It was assumed in the calculations that the value of A cannot be exceeded, both as a result of the action of a single turbulator and in the addition of values of the effectiveness of turbulators following one after another. This condition must also be satisfied in using the procedure described. If the change of effectiveness of turbulization with increasing z is such that at the location of any intensifier the value of the effectiveness exceeds the limit A, calculations are begun anew from this coordinate under the assumption that for this coordinate $f(\zeta) = A$, and there are no turbualtors upstream.

The form of the generalized relation for $f(\zeta)$ for the values of the empirical constants A, m, and n indicated above are shown in Fig. 3. The numbers alongside the points denote the model numbers. If lattice-intensifiers of two types were used in the models, primed numbers denote lattices of the second kind, and unprimed numbers denote lattices of the first kind. Equation (6) written for such models contains two unknown values of $f(\zeta)$. Therefore in obtaining data for Fig. 3, one of them (for the lattice with the larger value of ζ) was specified in accordance with Eq. (9), and the other was determined experimentally.

Returning to the data plotted in Fig. 2, we note the satisfactory agreement of the results obtained by the procedure of the present article and that of [4] for rod bundles with ordinary spacing lattices. Using the fact that the whole collection of such bundles is characterized by a rather narrow range of the relative distance between lattices, and assuming that the average value of l_d/d_h is 30, it follows from Fig. 2 that $f(\zeta) = 0.5$ for B = 20. This value corresponds to $\zeta = 0.22$ (see Fig. 3), which is very near the average value of the hydraulic resistance coefficients of ordinary spacing lattices.

TABLE 2. Experimental and Calculated Values of the Ratio of Critical Loads for Models (I-VII) with Lattice-Intensifiers to a Model with Regular RBMK-1000 Lattices

Ratio	I	II	III	IV	V	VI	VII
Experiment (E)	1,477	1,531	1,575	1,642	1,486	1,464	1,393
Calculation (C)	1,489	1,587	1,533	1,590	1,595	1,340	1,374
$\frac{E-C}{E}\cdot 100\%$	−0,8	−3,6	2,6	3,0	−7,3	8,5	1,3

It is also interesting to note that the increases in critical loads over those for an ideal bundle found by the procedure presented for fuel-element assemblies of the VVÉR and RBMK-1000 types turned out to be the same. It can be concluded from this that there is no need to question the possibility of using the IAE formula recommended earlier [3] to calculate critical loads in reactors of both types.

Thus, the computational procedure developed on the basis of experiments is characterized by the following basic parameters: $l_d/d_h = 14-42$; $\zeta = 0.285-1.015$; $p = 5.6-9.2$ MPa; $\rho w = 1150-3000$ kg/m^2·sec; $x = 0.22-0.85$. In using the procedure it is necessary to take account not only of the limitations indicated, but also of the possibility of applying the basic formula (4) under specific conditions.

LITERATURE CITED

1. V. Aden et al., in: Sixth Int. Heat Transfer Conf., Toronto, Aug. 7-11 (1978), Vol. 5, p. 41.
2. V. K. Ivanov and L. L. Kobzar', At. Energ., 49, 163 (1980).
3. V. S. Osmachkin, Preprint IAÉ-2345, Moscow (1974).
4. V. N. Smolin and V. K. Polyakov, in: Collection of Papers, Seminar TF-78 [in Russian], Vol. 2, Budapest (1978), p. 475.

BOILING OF COOLANT WITH DEPRESSURIZATION OF A HIGH-PRESSURE VESSEL

A. A. Avdeev
and V. K. Shanin

UDC 621.039.586

One of the main problems in computational-theoretical investigations of operational regimes of water-moderated water-cooled nuclear reactors under conditions of a loss-of-coolant accident is estimation of the degree of separation of coolant in the elements of the equipment in the first loop. The position of the true level and the steam content of the flow at the inlet to the discharge pipes to large extent determine the flow rate of the steam–liquid mixture through the location of the break, the dynamics of the pressure drop in the element examined, energy transfer under the protective envelope, as well as the residual coolant level at the end of the process. Several approximate methods for solving this problem have been developed up to now.

Two very simple models of the process were proposed previously in [1]: a model of complete separation of steam, and a uniform mixing model. In the first case it is assumed that the vessel contains a fluid level, on passage through which the steam content jumps from zero to one. In the second case it is assumed that the steam content inside the vessel is constant and there is no level (Figs. 1a, b). Such an approach was used in developong the well-known computer program "Tech'-12" [2]. In this program it was assumed that at the first stage of the accident the coolant is uniformly mixed, and then a level, caused by complete separation of coolant, is formed.

A semiempirical model of the process is used in the RELAP programs widely used abroad [3]. It is assumed that the vessel contains an interface between the steam and a two-phase mixture and that the steam content varies linearly within the mixture (Fig. 1c). The gradient of the steam content, as well as the rise velocity of bubbles, determining the steam content at the interface, were assumed to be constant. The values of these quantities were selected so that the computed pressure drop curves for the vessel studied coincided with the experimental data. However, the empirical constants introduced in this approach, to obtain good agreement with experiments, must vary with time as a function of the geometry of the vessel at the location of the leak [4].

In analogy to bubbling, it was assumed in [5] that the volume with the two-phase mixture contains a section with constant steam content and a transitional zone, within which the steam content increases linearly to unity (Fig. 1d). The steam content in the first section was determined in accordance with recommendations presented in [6], and the height of the transitional zone was determined from equations presented in [7].

Comparison of the models discussed with the experimental data [8, 9] shows that the existing procedures do not completely describe the nature of the experimental curves (Figs. 1e, f), and for this reason they have restricted applicability and limited accuracy.

A theory which permits calculating the distribution of the true volume steam content over the height of the vessel with boiling of the fluid due to the pressure drop is described in [10]. In the mathematical formulation it was assumed that the liquid and steam are in thermal equilibrium, that the pressure is the same at all points of the vessel, that the motion of the phases is one-dimensional and quasistationary, and that the group rise velocity of bubbles is constant over the height of the vessel. Comparison of the results of numerical solutions of the system of differential equations obtained with available experimental data gave good agreement. It was shown that at low pressure ($\rho'/\rho'' \to \infty$), when the fluid may be assumed to be stationary, the distribution of the true volume steam content over the height of the vessel satisfies the equation

$$\varphi_\infty = 1 - \exp(-H), \qquad (1)$$

Translated from Atomnaya Énergiya, Vol. 54, No. 6, pp. 399-404, June, 1983. Original article submitted June 15, 1982.

 0038-531X/83/5406-0406$07.50

where $H = h(\rho'/\rho'')\ (Q_v/wr)$ is the reduced distance from the bottom of the vessel; $Q_v = (-dp/d\tau) \times (di'/dp)$ is the equivalent intensity of internal heat sources. Here h is the dimensional distance from the bottom of the vessel; $dp/d\tau$, rate of decrease of pressure; w, relative rise velocity of the steam conglomerate; ρ', ρ'', density of the fluid and steam, respectively; r, specific heat of vaporization; and i', specific enthalpy of the saturated fluid.

An interpolation equation, generalizing the results of numerical solutions, was recommended for high pressures:

$$\varphi/\varphi_\infty = 1 + (\rho''/\rho')\,(\varphi_\infty/1 - \varphi_\infty). \tag{2}$$

We note that relations (1), (2) can also be used when the fluid boils as a result of internal liberation of heat, due to, e.g., radioactive decay or passage of electrical current through the fluid.

The following theoretical equation for determining the rise velocity of the steam conglomerate was presented in [11]:

$$\frac{(w - w_0)^2\,(w - \bar{w}'')^2}{w\bar{w}''} = g\delta\,(1 - \rho''/\rho'),$$

where

$$\delta = \begin{cases} 0.35\,(\rho'/\rho'')\,\sqrt{[\gamma/g(\rho' - \rho'')]} & \text{for} \quad \rho'/\rho'' \leqslant 150; \\ 60\sqrt{[\gamma/g\,(\rho' - \rho'')]} & \text{for} \quad \rho'/\rho'' > 150. \end{cases}$$

Here g is the acceleration of gravity; $\bar{w}''$, reduced velocity of steam; w_0, rise velocity of a single bubble; and γ, coefficient of surface tension.

For high steam loads, this equation has the asymptotic solution

$$w = a + \bar{w}'', \tag{3}$$

where $a = \sqrt{g\delta(1 - \rho''/\rho')}$.

The theoretical equation (3) gives good agreement with available semiempirical computational methods, e.g., in [6].

When the fluid boils due to the pressure drop, the reduced velocity of steam increases with distance from the bottom. In spite of this, the analysis in [11] leads to the conclusion that under these conditions the collective rise velocity w will remain constant over the height of the vessel. In accordance with [11], in this case w will be determined by the average steam content φ_{tw} over the height of the two-phase volume. Then, using the relation between the true volume steam content, the steam load, and the collective rise velocity, we can finally obtain from Eq. (3) a relation for calculating the rise velocity of the steam conglomerate:

$$w = a/(1 - \bar{\varphi}_{tw}). \tag{4}$$

In this paper we develop a method, based on relations (1) and (2), for calculating the nonstationary outflow of boiling coolant accompanying depressurization of the high-pressure vessel. The algorithm proposed is quite compact and does not lead to an appreciable increase in computer time, which is especially important for multielement computer simulations of reactor installations.

Let us single out, in the element of the power plant loop examined (reactor vessel, surge tank, etc.), a volume of steam V_s and a volume occupied by the two-phase coolant V_{tw}. Then the equations of conservation of mass and energy for the element examined will assume the following form [12] (it is assumed that the volume of the vessel examined is constant):

$$V\,(d/d\tau\,[\rho''\bar{\varphi} + \rho'\,(1 - \bar{\varphi})] = -G, \tag{5}$$

$$V(d/d\tau)[\rho''e''\bar{\varphi}+\rho'e'(1-\bar{\varphi})]=Q-i'G'-i''G'', \tag{6}$$

where V is the volume of the element ($V = V_S + V_{tw}$); $\bar{\varphi}$, fraction of the element volume occupied by steam; e', e", specific internal energy of the fluid and of the steam, respectively; i', i", specific enthalpy of the fluid and of the steam, respectively; Q, heat introduced into the element; G', G", outflow (inflow) of steam or fluid mass into the element, respectively; and $G = G' + G''$, total outflow (inflow) of coolant.

Taking into account the fact that the properties of the phases in the state of saturation are single-valued functions of pressure, we obtain from Eqs. (5), (6)

$$\frac{dp}{d\tau}=\frac{1}{V}\frac{(\rho''-\rho')C+GB}{(\rho''-\rho')A-B[\bar{\varphi}\,d\rho''/dp+(1-\bar{\varphi})\,d\rho'/dp]}; \tag{7}$$

$$\frac{d\bar{\varphi}}{d\tau}=\frac{1}{B}\left(\frac{C}{V}-A\frac{dp}{d\tau}\right), \tag{8}$$

where $A=\bar{\varphi}d(\rho''e'')/dp+(1-\bar{\varphi})\,d(\rho'e')/dp$; $B=\rho''e''+\rho'e'$; $C=Q-i'G'-i''G''$.

If we neglect the possible condensation of steam in the volume situated above the surface vaporization,* then the position of the two-phase coolant level can be determined from the equation of conservation of mass for the steam located in the steam volume:

$$(d/d\tau)(\rho''V_S)=I_S-G''_S, \tag{9}$$

where I_S is the flow of steam out of the two-phase volume into the steam volume through the evaporation surface; G''_S is the outflow (inflow) of steam from the steam volume:

$$\frac{dV_S}{d\tau}=\frac{1}{\rho''}\left(I_S-G''_S-V_S\frac{d\rho''}{dp}\frac{dp}{d\tau}\right). \tag{10}$$

The initial conditions for the system of ordinary differential equations (7), (8), and (10) at $\tau = 0$ have the form

$$p=p_0,\ \bar{\varphi}=\varphi_0,\ V_S=V_0. \tag{11}$$

We shall now determine the quantities I_S, G_S, G', G" on the right sides of the system of equations (7), (8), (10) (the heat inflow Q is assumed to be a known function of time and of the parameters in the vessel).

In accordance with the recommendations in [10],

$$I_S=\rho''\varphi_{le}wF, \tag{12}$$

where φ_{le} is the true volume steam content at the level of the evaporation surface; F is the area of the evaporation surface.

The relation between the quantities G', G" and G_S and the total flow rate of coolant through the location of the break is determined by the mutual position of the discharge pipe and the level of the two-phase coolant. We shall denote the mass steam content at the inlet to the discharge pipe by x and the mass fraction of steam captured from the steam volume by x_S. Then

$$G_S=x_SG,\ G''=xG,\ G'=(1-x)G.$$

*Under the conditions examined, this effect does not appreciably influence the results of the numerical calculations. To take it into account, the analysis should be performed based on a simultaneous solution of the equations of conservation of mass and energy written separately for the steam volume.

The nature of the change in the quantities x and x_s with the upper and lower position of the leak is obvious. When the discharge pipe is in a lateral position, if the level of the two-phase coolant is above the upper edge of the flow orifice,

$$\left.\begin{aligned} x &= \frac{\varphi_l \rho''}{\varphi_l \rho'' + (1-\varphi_l)\rho'}; \\ x_s &= 0 \end{aligned}\right\} \tag{13}$$

where φ_l is the true volume steam content at the level of the flow.

If, on the other hand, the coolant level is below the lower edge of the flow orifice then

$$x_s = x = 1. \tag{14}$$

The intermediate case, when the level of boiling coolant is located between the upper and lower edges of the flow orifice is most complicated. If it is assumed that there is no relative slipping of phases at the inlet to the discharge pipe x and x_s can be calculated using the following equations:

$$\left.\begin{aligned} x &= \frac{\varphi_s \rho''}{\varphi_s \rho'' + (1-\varphi_s)\rho'}; \\ x_s &= \frac{F_s \rho''/(F_s + F_{tw})}{\varphi_s \rho'' + (1-\varphi_s)\rho'}, \end{aligned}\right\} \tag{15}$$

where $\varphi_s = (\varphi_{le} F_{tw} + F_s)/(F_s + F_{tw})$ is the fraction of the flow-through cross section of the flow orifice occupied by steam; F_s, F_{tw} are the areas of the parts of the flow-through cross section of the flow lying above and below the evaporation surface, respectively.

The quantities φ_{le} and φ_l entering into relations (12), (13), (15) can be calculated from Eqs. (1) and (2), but it is difficult to use these relations directly due to the fact that the right side of Eq. (1) contains the rate of pressure drop sought $dp/d\tau$.

To avoid this difficulty, we shall determine the average steam content over the two-phase volume using the equation

$$\bar{\varphi}_{tw} = (V\bar{\varphi} - V_s)/(V - V_s). \tag{16}$$

In addition, this quantity can be obtained by integrating Eq. (2) over the height of the two-phase volume:

$$\bar{\varphi}_{tw} = 1 - 2(\rho''/\rho') + \frac{1}{H_{le}}[(\rho''/\rho')\exp H_{le} + (1-\rho''/\rho')\exp(-H_{le}) - 1], \tag{17}$$

where H_{le} is the reduced height of the level.

In deriving Eq. (17), it was assumed that the transverse cross section of the element is constant as a function of height. If equipment is present within the vessel, then Eq. (2) must be integrated taking into account the variability of the area of the flow-through cross section of the element.

In the range where $\rho'/\rho'' > 8$, which for water approximately corresponds to a saturation pressure of up to 13 MPa, Eq. (17) is approximated with sufficient accuracy by the dependence

$$\bar{\varphi}_{tw} \cong 1 - \exp(-0.5 H_{le}),$$

from which it follows that

$$H_{le} = -2\ln(1 - \bar{\varphi}_{tw}). \tag{18}$$

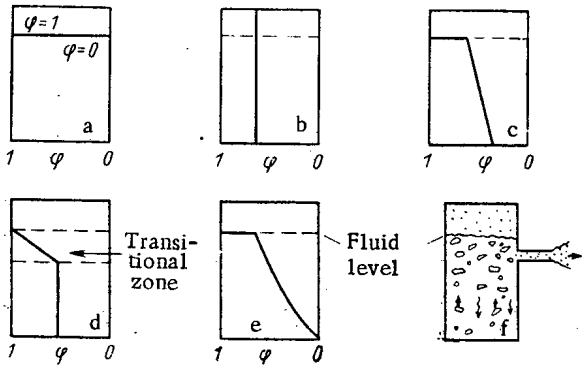

Fig. 1. Distribution of the true volume steam content as a function of height in the vessel: a) model of complete separation of steam; b) uniform mixing model; c) semiempirical RELAP model [3]; d) VTI model [5]; e, f) experimental data [8, 9].

Having calculated the value of $H_{\gamma e}$ from Eqs. (16) and (18), the reduced height of the position of the flow orifice can be determined as

$$H_{\gamma} = (h_{\gamma}/h_{\gamma e})\, H_{\gamma e}, \tag{19}$$

where h_{γ}, $h_{\gamma e}$ are the dimensional height of the position of the flow orifice and of the evaporation surface, respectively.

Using relations (18) and (19), the quantities φ_{γ}, $\varphi_{\gamma e}$, sought can be determined from Eqs. (1) and (2) at each step of numerical integration.

To close the mathematical description of the problem, the system of equations obtained must be supplemented by a relation that relates the flow rate of boiling coolant through the location of the break with the pressure in the vessel, steam content at the inlet to the discharge pipe, and its geometrical dimensions.

At the present time, well-founded methods for calculating the critical flow rate of boiling coolant have been developed only for a relatively narrow region of initial fluid parameters and geometrical dimensions of the channel [13]. For this reason, to check the proposed model, we use the results of only those experiments in which the flow rate of the outflowing coolant was measured while emptying the vessel [4, 8, 9, 14].

Available experimental data, e.g., [8, 9], show that at the time the leak appears, the pressure in the vessel drops sharply below the saturation curve. Then, within fractions of a second, the pressure is restored to a value close to the saturation curve. Subsequently, the boiling proceeds at equilibrium.

The initial stage of the decompression process (transition from unheated to metastable fluid) determines the dynamic action of shock waves on the elements of the installations within the housing. This phenomenon was analyzed theoretically by Avdeev et al. in [15].

In the present work the equilibrium stage of the process, during which most of the coolant is removed, is being analyzed. For this reason the initial conditions for Eq. (11) were given in the form

$$p = p_s(T_0),\ \bar{\varphi} = 0;\ V_s = 0. \tag{20}$$

It was noted in [8, 9], that the heat accumulated in the walls of the vessel had an appreciable effect on the distribution of the steam content over the height of the vessel. For this reason the inflow of heat from the walls and from the bottom of the vessel was included in the model of the regular cooling regime. In so doing, it was assumed that the temperature of the internal surface of the walls equals the saturation temperature, while the outer surface is adiabatically insulated. It was assumed that the initial temperature field is homogeneous. Comparison of the thermal flux computed in this manner with the results

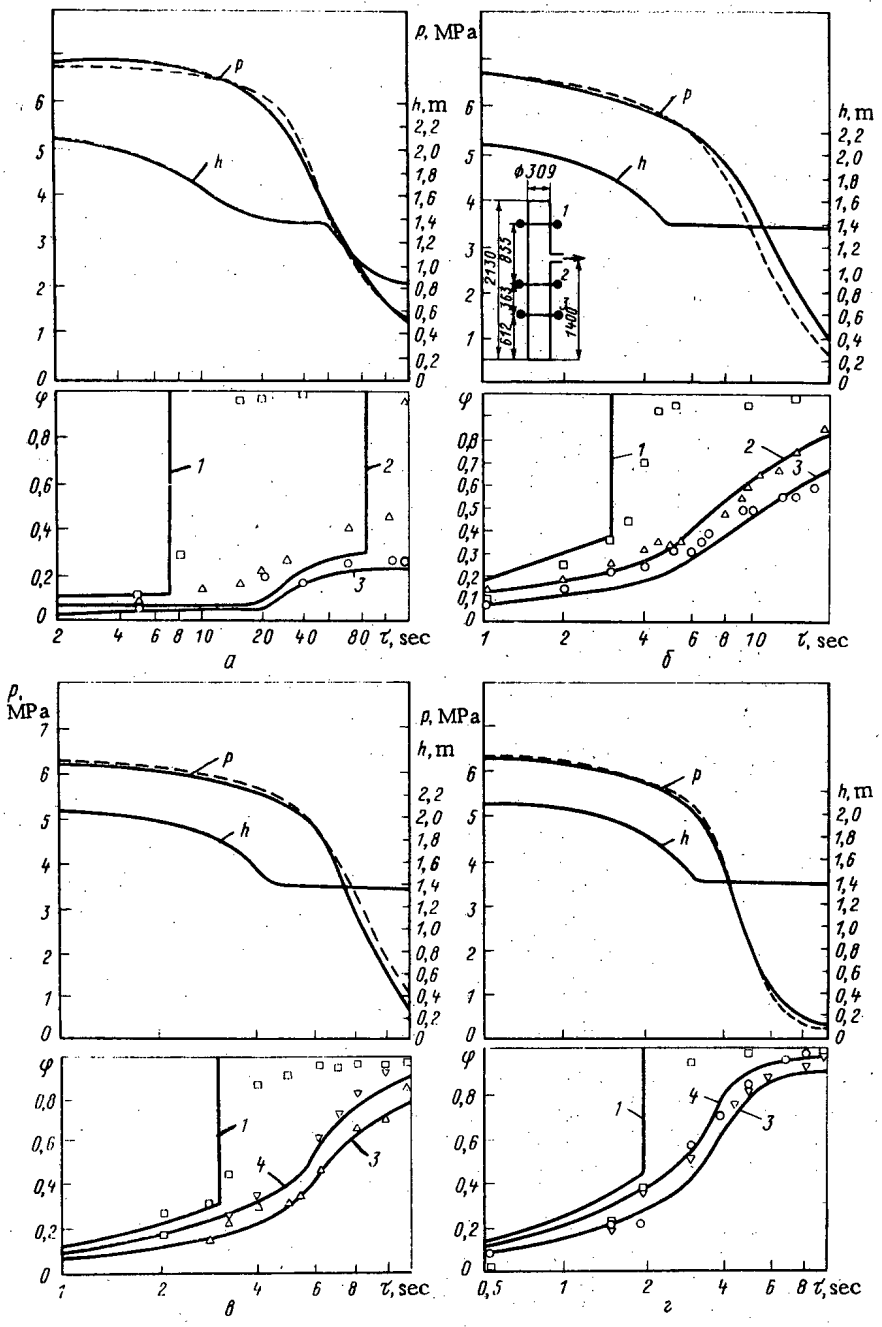

Fig. 2. Comparison of computed curves showing the pressure drop (p) and the level of the boiling coolant (h), as well as the distribution of the true volume steam content, with the experimental data of MÉI (---) [8, 9]. Leak diameter: 10 (a), 25 (b), 35 (c), 45 mm (d); change in steam content at the mark: 1830 (1), 975 (2), 612 (3), 1400 mm (4).

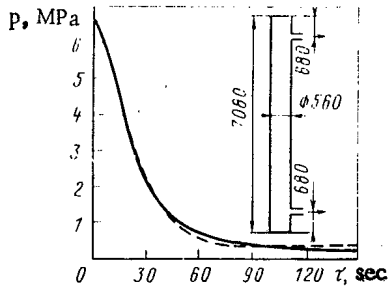

Fig. 3. Comparison of computed pressure drop curves with experimental data of ROSA (---). Diameter of upper orifice is 50 mm.

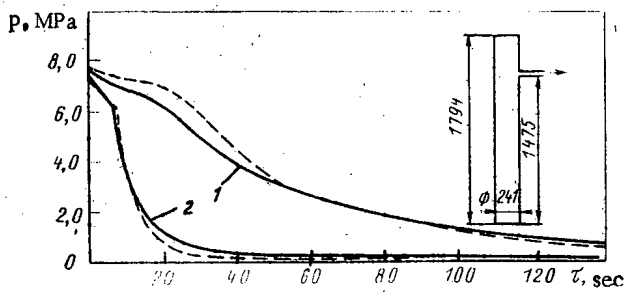

Fig. 4. Comparison of computer pressure drop curves with experimental data (---), obtained on the "Udar-1" stand; orifice diameter: 1) 5 mm; 2) 15 mm.

of the "exact" numerical solution of the one-dimensional nonstationary equation of heat conduction, performed with the use of the two-layer implicit six-point difference scheme (Crank–Nicholson scheme), gave good agreement for the conditions examined. We solved the system of ordinary differential equations (7), (8), (10) with the initial conditions (20) using the Runge–Kutta method with fourth-order accuracy. In performing the calculations, the thermophysical properties of phases, as well as their derivatives along the saturation curve, standing on the right side of Eqs. (7), (8), and (10), were fixed according to the data in [16].

The distribution of the true volume steam content over the height of the vessel when the vessel is depressurized was measured by Dement'ev et al. [8, 9] by the method of transillumination with rays. The change in mass of the two-phase coolant as a function of time was determined by integrating the steam content curve. The dimensions of the experimental vessel, as well as the location of the transilluminating setups, are shown in Fig. 2. The diameter of the leak was varied by restrictive diaphragms in the discharge pipe. It follows from a comparison with the experimental data in [8, 9] that there is satisfactory agreement not only with respect to pressure, but also with the distribution of the true volume steam content. Analogous results were also obtained for the other orifice diameters investigated (d = 5, 15, and 22 mm). We note that the maximum ratios of the area of the flow-through cross section of the flow orifice and the vessel volume used in the experiment in [8, 9] are several times larger than the corresponding values characteristic for modern reactor installations. The nature of the change in the true level of the coolant is interesting (see Fig. 2): When the upper edge of the orifice is attained, in spite of the continuing outflow of mass from the vessel, the fluid level remains constant for a long period of time. This phenomenon is characteristic for experimental vessels with a relatively high position of the discharge pipe.

Good agreement was obtained between the results of the calculation and the ROSA experiment [4], performed on a vessel with a large volume. In these experiments the flow rate was measured according to the hydrostatic pressure drop between the top and bottom of the vessel. The good agreement between the computed and experimental pressure curves occurred both with the upper and lower position of the flow orifice. The only exception was experiment No. 409 (upper orifice with diameter 70 mm, initial pressure 6.87 MPa). We note that a large disagreement between the measured flow rate curves and the results of theoretical estimates, made by Sobajima based on the RELAP-J program (Fig. 3), occurred only in this experiment.

In the experiments described in [14], the results of which are presented in Fig. 4, the coolant flow rate was determined with the use of a low-inertia strain system by weighing the volume studied during the course of the experiment. It is evident that the agreement is good.

Thus, the computational method developed permits including the "swelling" of the coolant level accompanying nonstationary boiling under pressure-drop conditions and gives good agreement with experiment. In addition, the universal nature of the recommendations in [10, 11] on which the present work is based, and the absence of empirical "adjustment factors", makes it possible to extend the analysis presented here to different coolants (organic fluids, heavy water, etc.). The use of the proposed procedure in multielement models does not appreciably complicate the numerical algorithm and does not appreciably increase the computer time required.

LITERATURE CITED

1. F. Moody, Transactions of the American Society of Mechanical Engineers, Ser. C, Heat Transfer, No. 1, 160 (1965).
2. V. P. Spasskov et al., Vopr. At. Nauki i Tekh. Ser., Dinamika Yad. Energet. Ustanovok, No. 1, 111 (1971).
3. C. Solbrig and D. Barnum, Nucl. Safety, 17, No. 2, 194 (1976).
4. M. Sobajima, Nucl. Sci. Eng., 60, 10 (1976).
5. A. M. Bukrinskii and R. L. Fuks, Teploenergetika, No. 9, 58 (1978).
6. D. A. Labuntsov, I. P. Kornyukhin, and É. A. Zakharova, ibid., No. 4, 62 (1968).
7. M. A. Styrikovich, O. I. Martynova, and Z. L. Miropol'skii, Steam Generation in Power Generating Plants [in Russian], Énergiya, Moscow (1969).
8. B. A. Dement'ev and Kh. M. Al'-Bakhili, Teploenergetika, No. 12, 72 (1978).
9. B. A. Dement'ev, Author's Abstract of Doctoral Dissertation, Technical Sciences, MÉI, Moscow (1977).
10. A. A. Avdeev and A. A. Avdeeva, Teploenergetika, No. 8, 53 (1980).
11. A. A. Avdeev, ibid., No. 3, 23 (1982).
12. M. E. Deich and G. A. Filippov, Gas-Dynamics of Two-Phase Media [in Russian], Énergoizdat, Moscow (1981).
13. D. A. Labuntsov and A. A. Avdeev, Teploenergetika, No. 9, 71 (1978).
14. V. N. Maidanik, et al., At. Energ., 47, No. 2, 117 (1979).
15. D. A. Labuntsov and A. A. Avdeev, Teplofiz. Vys. Temp., 20, No. 2, 288 (1982).
16. S. L. Rivkin and A. A. Aleksandrov, Thermophysical Properties of Water and Water Vapor [in Russian], Énergiya, Moscow (1980).

DETERMINATION OF THE YIELD FIGURES OF THE PRODUCTS RESULTING FROM THE ^{242}Pu AND ^{241}Am FISSION BY FAST NEUTRONS WITH THE AID OF SEMICONDUCTOR SPECTROMETRY

A. N. Gudkov, V. M. Zhivun,
A. V. Zvonarev, A. F. Zolotov,
A. B. Koldobskii, Yu. F. Koleganov,
V. M. Kolobashkin, S. V. Krivasheev,
and N. S. Piven'

UDC 539.173.8

Since the yield figures of the products resulting from the fission of transuranium nuclei, among them ^{242}Pu and ^{241}Am, by fast neutrons are increasingly used as nuclear constants in basic and applied work in nuclear physics and technology, the requirements to the accuracy and reliability of the yield figures become ever more stringent. To date, the results of measurements of the yield figures of the products resulting from the fission of ^{242}Pu by fast neutrons have been listed only in [1] for the heavy peak of the mass distribution. Furthermore, one of the two sets of yield figures of ^{242}Pu listed in [2] is a preliminary set without error estimates. This set does not allow specific conclusions on the experimental technique employed to obtain the data. The yield figures of the products resulting from the fission of ^{241}Am by fast neutrons were experimentally determined only in [2], but, as far as the method is concerned, that work is practically outdated. All this implies limitations in regard to the accuracy and reliability of the yield figures in view of the limited applicability of the experimental techniques used in [1, 2] and the large probability of systematic experimental errors influencing the final results. Furthermore, the list of the fission products considered in the cited papers is very limited.

In our work the yield figures of the fragment nucleides of ^{242}Pu and ^{241}Am were determined for the first time by semiconductor γ-spectrometry of an undivided mixture of fission products in an irradiated sample. This technique, which we used for the first time in investigations of the yield of the products of neutron-induced fission of other heavy nuclei [3-6], helps to substantially overcome the above-indicated difficulties in the evaluation of the research work.

The samples of the material to undergo fission were irradiated in the center of the BR-1 reactor core (FÉI). The neutron flux density at the point of irradiation was $6 \cdot 10^{10}$ neutrons/(cm^2 · sec). The samples were ^{242}Pu and ^{241}Am dioxides compacted and hermetically sealed in 4-mm-high cylindrical steel shells with a diameter of 6 mm. The wall thickness was about 0.15 mm (Table 1). The mass concentration of the impurities in the samples did not exceed 0.1%.

Measurements on the irradiated samples were made with a semiconductor γ-spectrometer of standard design with a DGDK-32A Ge(Li) detector having a resolution of 3.5 keV for the 1333 keV ^{60}Co radiation. The spectrometer was calibrated with the aid of an OSGI set and

TABLE 1. Characteristics of the Samples of the Materials Undergoing Fission

Sample	Pure mass of the material undergoing fission	Irradiation time, h
^{242}Pu (first)	84,1	7,23
^{242}Pu (second)	72,6	1,00
^{241}Am	54,5	4,00

Translated from Atomnaya Énergiya, Vol. 54, No. 6, pp. 404-406, June, 1983. Original article submitted August 2, 1982.

 0038-531X/83/5406-0414$07.50

TABLE 2. Yield of the Products Resulting from the Fission of ^{242}Pu and ^{241}Am by Fast Neutrons

Fission products	^{242}Pu		^{241}Am	
	our work	[1]	our work	[2]
^{85m}Kr	0,37±0,04		0,87±0,18	
^{87}Kr	1,47±0,23		0,91±0,23	
^{88}Kr	0,77±0,10		1,80±0,41	
^{89}Sr				1,20±0,10
^{91}Sr	1,77±0,14		2,13±0,21	1,90±0,05
^{92}Sr	1,93±0,11		2,89±0,18	
^{92}Y	2,15±0,25			
^{93}Y	3,32±0,60			3,00±0,20
^{94}Y			2,71±0,28	
^{95}Zr	3,24±0,38			2,70±0,10
^{97}Zr	4,78±0,32		5,47±0,27	
^{99}Mo				6,3±0,3
^{103}Ru				7,7±0,2
^{104}Tc	5,52±0,55		5,35±0,83	
^{105}Ru	6,92±0,43			6,6±0,2 *
^{105}Rh	7,48±0,47			
^{111}Ag				0,22±0,11
^{125}Sb		0,059±0,009		
^{125}Sb		0,050		
^{128}Sn	0,63±0,41		0,67±0,08	
^{129}Sb	2,23±0,74		1,76±0,42	
^{130m}Sb	0,71±0,07		1,11±0,08	
^{131}Sb			1,97±0,30	
^{131m}Te	0,41±0,06		1,25±0,29	
^{131}I	3,19±0,21			2,1±0,1
^{131}Xe		3,16±0,19		
^{131}Xe		3,32		
^{132}Te			4,46±0,60	
^{132}I	4,64±0,38			
^{132}Xe		4,59±0,28 *		
^{132}Xe		4,52		
^{133}I	7,04±0,42		7,16±0,56	4,0±0,2
^{133}Cs		6,97±0,42		
^{133}Cs		6,49		
^{134}Te	6,75±0,78		5,44±0,40	
^{134}I	6,83±0,38		5,30±0,36	
^{134}Xe		7,59±0,46		
^{134}Xe		7,36		
^{135}I	6,83±0,38		5,30±0,36	4,8±0,3
^{135m}Xe			2,21±0,55	
^{135}Xe	6,99±0,41		6,61±0,40	
^{135}Xe†			0,20±0,02	
^{135}Cs		7,13±0,43		
^{135}Cs		6,89		
^{136}Cs ‡				0,16±0,08
^{136}Cs		6,56		
^{137}Cs		6,46±0,39		5,6±2,8
^{137}Cs		6,21		
^{138}Cs			4,42±0,48	6,4±0,4
^{138}Cs †			0,19±0,10	
^{138}Ba		6,28±0,38		
^{139}Ba	5,87±0,37		6,72±1,14	
^{139}La		5,99±0,36		
^{140}Ba	6,70±0,69		4,82±0,45	5,2±0,1
^{140}La	6,49±0,78		5,62±0,59	
^{140}La †			0,020±0,006	
^{140}Ce		4,95±0,30		
^{141}Ce				4,7±0,2
^{142}La	4,63±0,37		4,04±0,24	
^{142}Ce		4,58±0,27		
^{143}Ce	3,95±0,30		3,75±0,40	
^{143}Nd		4,65±0,28		
^{143}Nd		4,52		
^{144}Ce				3,2±0,2
^{144}Nd		4,32±0,26		
^{144}Nd		4,16		
^{145}Nd		3,43±0,21		
^{145}Nd		3,38		
^{146}Nd		2,94±0,18		
^{146}Nd		2,92		
^{147}Sm		2,40±0,14		
^{148}Nd		2,03±0,12		
^{148}Nd		1,98		
^{149}Nd	1,51±0,14			
^{149}Sm		1,62±0,09		
^{149}Sm		1,64		
^{150}Nd		1,33±0,08		
^{150}Nd		1,32		
^{151}Sm		1,00±0,06		
^{151}Sm		1,05		
^{152}Sm		0,770±0,046		
^{152}Sm		0,84		
^{154}Sm		0,43±0,026		
^{154}Sm		0,48		

*Normalized yield figures.
†Relative independent yield figures.
‡Absolute independent yield figures.

a ^{226}Ra source in equilibrium with the daughter product of the decay; the technique of [7] was employed. In order to reduce the level of the intense intrinsic background of the ^{241}Am 60 keV radiation, a 2-mm filtering lead screen was used in the measurements. The optimum filter thickness was chosen so that the background of the spectrometer was reduced to 3-4% of the "alive" time. The filters were also employed when the luminous yield of the spectrometer was calibrated. The γ-radiation spectra of the irradiated samples were processed with SM-3 and SM-4 computers with the technique described in [8]. The half-life periods and the absolute quantum yield of the γ-radiation of the fission products were selected in accordance with [9].

Certain values, which are equal to the yield figures with an accuracy of a constant coefficient and which must be normalized, are the final results of the processing of the primary experimental information obtained with our technique. Absolute normalization is not possible in this case, because the number of fissions in the sample cannot be determined with acceptable accuracy. We therefore used in the present work a relative normalization which is based on the selection of a certain "fast" yield figure as a reference value in a particular fission process. Though the design of the BR-1 reactor allows monitoring irradiations in the thermal column, normalization performed with the classical R method does not provide significant advantages over the method described, because the error fraction which in the final results originates from the yield figures of the reference fission product and the fission product under inspection in the ratios of the R method (e.g., in the fission of ^{235}U by thermal neutrons) is in this case comparable with the error caused by uncertainties in the absolute quantum yields and calibration errors of the spectrometer. The overall work volume is doubled when the R method is employed.

The selection of the reference nuclides was guided by the following concepts:

The characteristic decay values (half life and absolute quantum yield of the γ-lines recorded) must be known with a high degree of accuracy and reliability;

the errors of the known yield figures of the reference fission products, as well as the relative value obtained in the experiments described, must be as small as possible.

Based on the above criteria, we used as reference fission products ^{132}Xe (yield figure 4.59 ± 0.28) in the case of ^{242}Pu and ^{105}Ru (6.6 ± 0.2) in the case of ^{241}Am. The errors which are made in the determination of the yield figures of the fission products are caused by the statistics of the measurements (1-15%), by uncertainties in the reference values of the yield figures (6.1% and 3% for ^{132}Xe and ^{105}Ru, respectively), by the calibration of the spectrometer with respect to its efficiency (1-3%), and by the handbook values of the absolute quantum yields ($\sim$3%). The results of the measurements, along with the data of [1, 2], are listed in Table 2.

The following conclusions can be drawn from an analysis of the results listed in Table 2.

The yield figures which we obtained for the fission products of ^{242}Pu are in good agreement with the results of [1] (except for the mass 140). This means that a successful selection of the normalization had been made. In our opinion, the systematic error of [1] or an editorial error made in the preparation of the paper is the most likely reason for the discrepancy of the yield figures for $A = 140$. In the present work the probability of a systematic error is extremely small, because, first of all, good agreement between the cumulative yield figures of the two members of the chain of $A = 140$ (^{140}Ba and ^{140}La) was obtained, and, secondly, the absolute quantum yields of the γ-radiation, which have the greatest bearing upon the systematic errors of the technique employed for ^{140}Ba and ^{140}La, are known in very reliable form.

The general agreement between the yield figures obtained for ^{241}Am and the data of [2] is satisfactory. As in the case of ^{242}Pu, the agreement means that the normalization was successfully selected. Both the error of the individual yield figures and the discrepancy between the results of the papers cited substantially exceed the errors of the case of ^{242}Pu. Final sets of yield figures for the products of ^{241}Am fission by fast neutrons can be stated only after further experimental investigations for the purpose of: 1) increasing the precision of individual measurements (this is particularly necessary in cases in which the differences between the results of the present work and the data of [2] are significant, as, e.g., in the case of ^{133}I and ^{135}I); 2) establishing systematic errors; 3) expanding the available experimental information.

LITERATURE CITED

1. J. Cuninghame, in: Proc. 11th Advisory Group Meeting on Fission Product Nuclear Data, Petten, 1977, Vol. 1, p. 351, Vienna (1978).
2. R. Richard, C. Goeking, and F. Wyatt, Nucl. Sci. Eng., 23, 115 (1965).
3. A. N. Gudkov et al., Neutron Physics, Reports of the 4th All-Union Conf. on Neutron Physics [in Russian], Kiev, 1977; Moscow, Press of the Central Scientific Inst. of Atomic Information, Part 3, p. 192 (1977).
4. A. A. Byalko et al., in: Experimental Techniques of Nuclear Physics [in Russian], No. 3, Atomizdat, Moscow (1978), p. 82.
5. A. N. Gudkov et al., in: Experimental Techniques of Nuclear Physics [in Russian], No. 4, Atomizdat, Moscow (1978), p. 105.
6. A. N. Gudkov et al., At. Energ., 48, No. 6, 401 (1980).
7. V. V. Kovalenko and V. M. Kolobashkin, in: Experimental Techniques of Nuclear Physics [in Russian], No. 6, Atomizdat, Moscow (1980), p. 70.
8. A. N. Gudkov et al., in: Experimental Techiques of Nuclear Physics [in Russian], No. 6, Atomizdat, Moscow (1980), p. 81.
9. J. Blachot and C. Fiche, At. Nucl. Data Tabl., 20, 241 (1977).

EFFECTS OF NEUTRON IRRADIATION ON THE FAILURE VISCOSITY OF GRAPHITE

L. L. Lyshov, V. N. Barabanov, Yu. S. Virgil'ev,
O. K. Chugunov, and A. I. Plavskii

UDC 666.764.4:
620.178.74

The working conditions in power systems require research on the failure mechanics of the graphite materials used. There are radiation-induced changes in the ultimate strength and elastic modulus of graphite [1], which indicate a reduction in the plasticity and an increase in the probability of brittle failure similar to those observed for metals [2]. Although neutron irradiation increases the impact viscosity of graphite [3] and the cracking resistance [4], it is nevertheless very important to examine the characteristics of the failure mechanics under conditions of high-temperature irradiation.

Here we present results on the critical stress intensity K_{IC} for a wide range of graphite materials after neutron irradiation at various temperatures. The physicomechanical, structural, and certain technological characteristics of these graphites made by the electrode technology are given in Table 1.

Specimens used for failure-viscosity testing (Fig. 1) were made of graphites ARV-2, VPP, MPG-8, and PROG-2400, which were irradiated in tube devices replacing fuel-pin assemblies in a VVR research reactor [1] with irradiation temperatures of 343-353°K and exposure up to a fluence of 3×10^{20} neutrons/cm^2 (here and subsequently, the neutron energy was over 0.18 MeV).

The specimens of reactor graphite and PGG graphite were cut with a special tubular saw from blocks of graphite column and the reflector in the MR reactor [1]. Tests were done on specimens of reactor graphite cut from blocks 1, 2, and 4 [1], which had been irradiated to a fluence of $(0.8\text{-}1.0) \times 10^{21}$ neutrons/cm^2 at 573°K, to $(2.8\text{-}3.6) \times 10^{21}$ neutrons/cm^2 at 773°K, and to $(5.3\text{-}7.2) \times 10^{21}$ neutrons/cm^2 at 973°K, correspondingly. The specimens cut from a reflector block (PGG graphite) were irradiated to a fluence of 0.5×10^{20} neutrons/cm^2 at 373-473°K.

The failure-viscosity tests were performed by the eccentric stretching technique on rectangular and disk specimens. The main advantage of this scheme is that one can use compact specimens, which is particularly important in view of the restricted dimensions of the irradiation tubes. Also, the fairly large working cross section (10 × 20 mm) enabled us to test specimens of coarse-grained PROG-2400 graphite and reactor graphite without introducing errors associated with the scale factor. The tests were performed with a Tsvik-1474 machine with the diagram recorded in P—v coordinates, where P is load and v is displacement at the point of load application. The errors of measurement for the load and displacement were not more than ± 1%. The critical stress intensity coefficient at the instant of crack propagation was calculated from

$$K_{IC} = \frac{P_c \sqrt{l}}{tb} Y_{1,2}, \qquad (1)$$

where

$$Y_1 = 29.6 - 185\left(\frac{l}{b}\right) + 655\left(\frac{l}{b}\right)^2 - 1017\left(\frac{l}{b}\right)^3 + 639\left(\frac{l}{b}\right)^4;$$

$$Y_2 = 29.6 - 162\left(\frac{l}{b}\right) + 492\left(\frac{l}{b}\right)^2 - 663\left(\frac{l}{b}\right)^3 + 405\left(\frac{l}{b}\right)^4$$

are the K calibration coefficients for specimens of rectangular and disk shapes, correspondingly; P_c, crack propagation load; t, b, thickness and width of the specimen; and l, length of the initial notch (b and l are measured on the line of centers for the holes in the specimen, see Fig. 1). In view of the linearity of the failure diagrams, K_{IC} was calculated for $P_c = P_{max}$. After the failure viscosity tests, rectangular plates of size 3 × 3 × 25 mm were cut from half of the specimen to measure the dynamic elastic modulus by a resonant method employing push-wave vibrations. The error in measuring E by this method is not more than 10%.

Translated from Atomnaya Énergiya, Vol. 54, No. 6, pp. 406-409, June, 1983. Original article submitted July 9, 1982.

 0038-531X/83/5406-0418$07.50

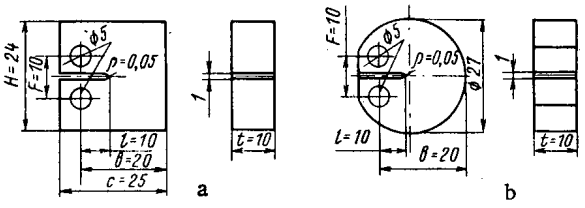

Fig. 1. Rectangular (a) and disk (b) specimens for testing for failure viscosity in eccentric stretching.

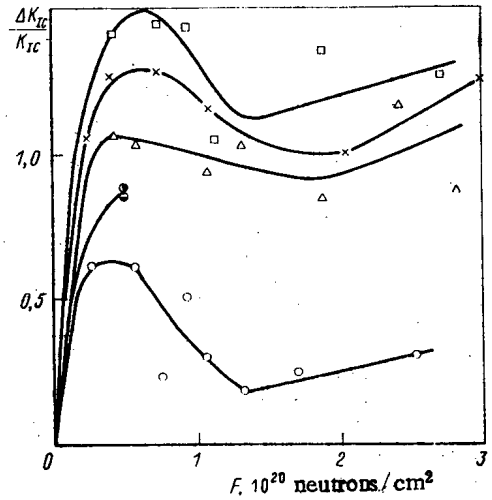

Fig. 2. Dependence of the relative change in K_{IC} on fluence for graphites ARV-2 (□), PROG-2400 (×), VPP (Δ), PGG (◑, ◒ — specimens cut parallel and perpendicular to pressing axis), and MPG-8 (○). Specimens of graphites ARV-2, PROG-2400, VPP, and MPG-8 were cut perpendicular to the pressing axis and were irradiated at 343-353°K, while the PGG specimens were irradiated at 373-473°K.

Figures 2 and 3 show the relative changes in the critical intensity coefficient and dynamic elastic modulus, correspondingly, for specimens of five grades of graphite irradiated to fluences of 3×10^{20} neutrons/cm^2. On account of the restricted tube volume, each point in Figs. 2 and 3 corresponds to data for four specimens of the materials ARV-2, PROG-2400, VPP, and MPG-8. The irradiation temperature range was 343-353°K. At 373-473°K we irradiated 10-12 specimens of PGG graphite cut from a reflector block in two directions. The coefficient of variation K_{IC} for PGG specimens cut in the parallel direction was not more than 8%, as against 10% for ones cut in the perpendicular direction. Figure 4 shows the dependence on neutron fluence for the relative change in K_{IC} for reactor graphite. Table 2 gives the absolute values of K_{IC} and E and also the results from statistical processing. Each point in Fig. 4 characterizes the data from 10-12 specimens; $\alpha = 0.9$ in deriving the confidence range for the mean.

As the curves in Figs. 2 and 3 are similar in shape, and in view of the results of [4], one naturally supposes that the variation in K_{IC} as the fluence increases is due to change in the elastic parameters and strength ones. In turn, the increases in the elastic modulus and strength are associated with the blocking of mobile dislocations at radiation point defects in the basal plane [1, 5, 6].

There are peaks on the curves for the elastic modulus at a fluence of $(0.3\text{-}1.0) \times 10^{20}$ neutrons/cm^2, which is due to the start of linkup between interstitial atoms into groups, with increase in the distances between them [1, 6]. This is characteristic of the elastic modulus in a carbon material on neutron irradiation at low temperatures (up to 500°K). The effect is the more pronounced the higher the degree of ordering or graphitization [1]. This indicates that the radiation defects have different effects on the two structural components of graphite: the graphitized grains of coke filler and the coke from the bonding agent.

Radiation point defects in the crystallinity zones in the filler coke grains cause changes in the properties, in particular, elastic modulus and strength, larger than those

TABLE 1. Physicomechanical, Structural, and Technological Characteristics of Graphite

Material	Fired coke and sinter			Unfired coke and sinter	Fired coke and sinter	
	ARV-2	PROG-2400	VPP	MPG-8	Reactor graphite	PGG
Formation method	Pressing	Extrusion	Pressing	Pressing	Extrusion	Pressing
Density*, ton/m^3	1,51–1,58	1,58–1,64	1,81–1,88	1,83–1,86	1,68–1,72	1,70–1,75
Porosity*, m^3/ton	0,161–0,219	0,108–0,162	0,075–0,104	0,073–0,083	0,125–0,160	
Maximum grain size, mm	0,15	2,3	1,2	0,15	2,3	1,2
Coke residue from bonding agent, %	21	15–17	17–19	28	15–17	14–16
Tensile strength, MPa	6,55(4,7–8,4)	9,0(8,0–10,7)† / 6,0(4,5–7,2)	13,5(10,4–17,7)	28,0(22,7–33,7) / 27,5(25,1–30,9)	9,0(6,5–10) / 7,0(5,0–10,0)	
Compressive strength, MPa	26,5(22,5–30,5)	32,0(31,0–34,5) / 29,0(28,0–30,2)	69,0(65,0–72,0)	88,5(76,4–98,6) / 96,0(87,7–107,6)	33,0(31,0–40,0) / 33,0(26,0–45,5)	56,0 / 58,0
Elastic modulus (dynamic)*, 10^4 MPa	0,50(0,47–0,53)	0,53(0,50–0,55)	0,96(0,93–0,99)	1,31(1,22–1,40)	0,72 / 0,68	—
Critical stress intensity coefficient*, 10^{-4} MPa·m$^{1/2}$	4,19(3,56–4,82)	4,09(3,27–4,91)	8,87(8,06–9,68)	13,40(12,21–14,59)	6,11(5,18–7,04) / 6,08(5,09–7,07)	9,40(8,22–10,58) / 9,27(8,15–10,39)

*These characteristics were determined in this study, and the others have been taken from the handbook "Properties of Carbon-Based Constructional Materials" [in Russian], Metallurgiya, Moscow (1976).

†The top line is for speciemens cut in the parallel direction and the bottom line for ones in the perpendicular one; in other cases the specimens were cut in the perpendicular direction.

Declassified and Approved For Release 2013/02/06 : CIA-RDP10-02196R000300020006-4

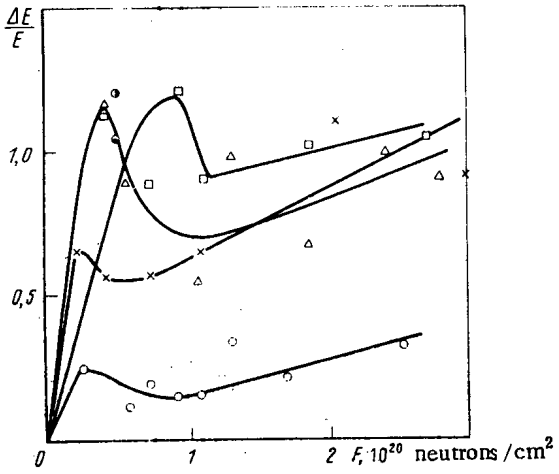

Fig. 3. Dependence of the relative change in elastic modulus on fluence (symbols as in Fig. 2).

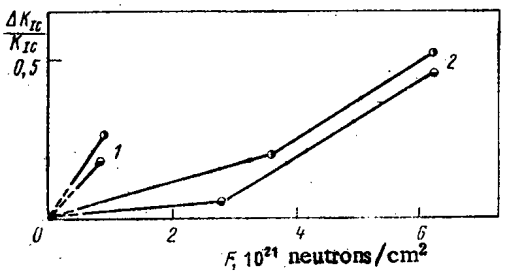

Fig. 4. Dependence of the relative change in K_{IC} for reactor graphite on fluence at 573 (1) and 773-973°K (2): ◑, ◒) parallel and perpendicular specimen cutting, correspondingly.

TABLE 2. Critical Stress Intensity Coefficient and Dynamic Elastic Modulus for Specimens of Reactor Graphite after Neutron Irradiation

Characteristic	Fluence, 10^{21} neutrons/cm²			
	0	0,8–1,0	2,8–3,6	5,3–7,3
Irradiation temperature	293	573	773	973
Critical stress intensity coefficient, 10^{-1} MPa·m$^{1/2}$	6,11±0,93 * 6,08±0,99	7,79±1,18 7,26±0,59	7,35±0,78 6,39±1,27	9,37±1,21 8,96±0,74
$\Delta K_{IC}/K_{IC}$	–	0,27/0,29	0,20/0,05	0,53/0,47
Dynamic elastic modulus, 10^4 MPa	0,72±0,11 0,68±0,06	1,38±0,21 0,91±0,08	1,34±0,14 0,87±0,16	1,28±0,16 1,12±0,09
	–	0,92/0,34	0,87/0,28	0,78/0,64

*Top line, specimens cut in the parallel direction; bottom line, in the perpendicular one.

in the graphite from the binder coke. This is due to the higher porosity and stratification of the graphite from the latter. For the same reasons, when the interstitial atoms begin to link up into groups (at a fluence of about $(0.3\text{-}1.0) \times 10^{20}$ neutrons/cm^2), the relative reduction in the elastic modulus occurs mainly in the filler coke grains. The variations in the properties of the material as a whole (Figs. 2, 3) result from superposition of these changes in the grains and in the graphite from the bonding-agent coke. It cannot be said that the grains are entirely zones of ideal crystallinity, while the graphite from the bonding coke is completely stratified. The division is nominal, but it relates to the predominance of the zones, and one cannot deny that there are zones of crystallinity in the grains and zones of stratification in the graphite from the bonding-agent coke.

The following evidence also confirms this. The largest relative increase in E and K_{IC} at a fluence of $(0.5\text{-}0.8) \times 10^{20}$ neutrons/cm^2 occurs (Figs. 2, 3) with ARV-2 and PROG-2400 graphites, which are based on fired coke and which have smaller amounts of coke residue from the bonding agent (about 15-20%; see Table 1). Conversely, MPG-8 graphite based on unfired coke has the highest amount of coke residu from the bonding agent (about 28%), and this shows the least relative increase in these characteristics.

Therefore, this study of the cracking resistance in relation to neutron fluence has shown that:

1. On low-temperature irradiation (373-473°K) at a fluence of $\leq 3 \cdot 10^{20}$ neutrons/cm^2, the cracking resistance (K_{IC}) for graphite ARV-2, MPG-8, PROG-2400, and VPP increases by 100-150%, while reactor graphite irradiated to a fluence of 7.2×10^{21} neutrons/cm^2 at 573-973°K shows an increase of only 20-50%.

2. The increase in resistance and in the strength characteristics is derived from a dislocation mechanism, in which the motion of dislocations in the basal plane is prevented mainly by point defects arising from the irradiation (interstitial atoms and groups of these).

3. There is less increase in the cracking resistance as the irradiation temperature rises, mainly on account of point-defect annealing (diffusion) and the formation of complexes.

An explanation is provided for the behavior of these characteristics on low-temperature irradiation in the fluence range $(0.03\text{-}.0) \times 10^{20}$ neutrons/cm^2 on the basis of the assumption that there are different effects from the radiation defects in the graphitized grains of filler coke and in the graphite from the bonding-agent coke.

LITERATURE CITED

1. V. V. Goncharov et al., The Effects of Irradiation on Reactor Graphite [in Russian], Atomizdat, Moscow (1978).
2. A. Bement, R. Hoeland, and F. Smith, in: Failure [Russian translation], Vol. 3, Mir, Moscow (1976), p. 579.
3. Yu. S. Virgil'ev, V. V. Gundorov, and V. G. Makarchenko, At. Energ., 42, No. 5, 416 (1977).
4. S. Sato et al., At. Energy Soc., 21, No. 12, 957 (1979).
5. R. Taylor et al., Carbon, 5, No. 5, 519 (1967).
6. I. Mason and R. Knibbs, ibid., p. 493.

SEPARATION OF HYDROGEN ISOTOPES H_2—HT AND D_2—DT BY ADSORPTION ON NaA SYNTHETIC ZEOLITES

I. A. Alekseev, I. A. Baranov,
V. A. Novozhilov, G. A. Sukhorukova,
and V. D. Trenin

UDC 621.039.3:546.11.02

The development of nuclear power generation has brought forth the problem of localizing tritium, a heavy radioactive isotope of hydrogen, which is formed in large quantities during the operation of heavy-water nuclear reactors and is accumulated in the effluents of enterprises that process used nuclear fuel. According to the data of IAEA, by the year 2000 up to $2 \cdot 10^{19}$ Bq of tritium will be produced in the form of such wastes annually, which is tens of times as high as the natural rate of formation of tritium on earth. A thermonuclear reactor of equivalent power, according to estimates, can produce 10^4-10^5 times as much tritium as an atomic power station [1].

The problem of trapping and concentrating tritium can be solved by using various methods of hydrogen-isotope separation: rectification of water [2], two-temperature exchange between water and hydrogen sulfide [3], sorption by palladium [4], etc. The only present-day industrial plant for producing tritium from heavy water and concentrating it is in operation in France and is based on the combined method of isotope exchange between water and hydrogen and rectification of hydrogen isotopes [5].

A promising method for the separation of isotope varieties of hydrogen is the sorption of molecular hydrogen on synthetic zeolites. In the investigation of the water—zeolites system it was found [6] that the heavy isotopes are sorbed preferentially on zeolites and that NaA zeolite has the highest selectivity for hydrogen isotopes; equilibrium in the system is established rapidly, and the separation factors have relatively high values. However, the experiments were conducted with stable hydrogen isotopes. Except for [7], in which the separation factors were determined by a chromatographic method at a relatively high temperature (~200°K), and which is of no practical significance for the separation of hydrogen isotopes, there are no published data concerning the separation factors of tritium-bearing varieties of hydrogen isotopes when they are adsorbed on NaA zeolite.

The purpose of the present study is to determine the separation factors for H_2—HT and D_2—DT separation on NaA zeolite. We investigated granular zeolites whose granule dimension is 1.5-2 mm. The H_2—HT and D_2—DT mixtures were obtained by using metallic lithium to decompose water of the proper isotopic composition. The tritium content of the gas was $4 \cdot 10^{-8}$ at.%. The experiments were carried out on an apparatus with forced gas circulation, analogous to the one described in [4]. Before the experiment the zeolite was pumped out to a pressure of 1 Pa, with heating up to 670°K.

Liquid nitrogen and liquid air were used as cooling liquids in the sorption of hydrogen. When the gas was circulated through a cooled cell with the zeolite, isotopic equilibrium was established after about 20 min. After taking samples of the gaseous medium for isotope analysis, the cell was closed and the gas was pumped out from the rest of the apparatus to a pressure of 1.3 Pa. Thereafter, at 300°K, the hydrogen was desorbed from the zeolite, and after mixing with a circulation pump, the desorbed gas was analyzed. The analysis was carried out with the aid of an LKhM-8 MD chromatograph and a flow-through proportional counter. In the determination of the separation factor for H_2—D_2 the temperature of the chromatographic column was 77°K, and the chromatograph recorded separate H_2 and D_2 peaks. In the determination of the separation factors for H_2—HT and D_2—DT the column was at room temperature. Under these conditions the chromatograph recorded one peak, whose area corresponded to the amount of hydrogen removed for analysis and was calculated by means of an I-02 integrator with an error of 0.5%.

Translated from Atomnaya Énergiya, Vol. 54, No. 6, pp. 409-411, June, 1983. Original article May 28, 1982.

0038-531X/83/5406-0423$07.50

TABLE 1. Separation Factors of Hydrogen Isotopes in a System Consisting of Hydrogen and NaA Zeolites

Temperature, °K	Isotope varieties		
	$H_2 - D_2$	$H_2 - HT$	$D_2 - DT$
77,6	2,55±0,06	1,84±0,06	1,29±0,04
87,3	—	1,78±0,06	1,23±0,03

At the outlet of the chromatograph the carrier gas with the hydrogen sample was mixed with the counter gas, which in this case was a mixture of propane and butane, and entered an internally filled counter. The number of pulses recorded by the counter, which was proportional to the amount of the radioactive component passed through the counter, was calculated by a PP-9 converter. With this kind of analysis system it is possible to determine the separation factors of the stable and radioactive isotope varieties of hydrogen molecules with an error of 3%.

The separation factors α were calculated as the ratio of the relative concentrations of the relevant isotopic varieties of hydrogen in the desorbed gas and in the gaseous phase. We introduced a correction for the dilution of the desorbed gas by hydrogen with an equilibrium isotopic composition, which was left before desorption in the free volume of the cell with the zeolite.

The results of the measurements are shown in Table 1. The values given are averages obtained from a series of measurements and are given with a confidence probability of 95%. The measurements were carried out at a gaseous-phase pressure of 20-100 kPa, corresponding to a sorbent filling of 70-100 neutrons $\cdot$ cm^3/g. In this region of filling, the separation factor is practically constant [6]. We discovered that α depends (within the limits of measurement error) on the sorbent filling in the region investigated. The determined value $\alpha_{H_2-D_2}$ at 77.6°K corresponds to published data, which indicates the reliability of the method. The values we found for α_{H_2-HT} and α_{D_2-DT} are fairly high and exceed the analogous separation factors in the rectification of liquid hydrogen. Thus, we have a theoretical possibility of concentrating tritium by the method of adsorption on NaA zeolite at a higher temperature (in comparison with hydrogen rectification) and with lower energy consumption. In comparison with the other adsorption system (the hydrogen–palladium system), the hydrogen–zeolites system has a much lower sorbent cost.

LITERATURE CITED

1. L. A. Lenskii, Physics and Chemistry of Tritium [in Russian], Énergoizdat, Moscow (1981).
2. Ya. D. Zel'venskii et al., At. Energ., 36, No. 5, 396 (1974).
3. B. M. Andreev, Ya. D. Zel'venskii, and V. V. Uborskii, ibid., 44, No. 3, 240 (1978).
4. B. M. Andreev, A. S. Polevoi, and A. N. Perevezentsev, ibid., 45, No. 1, 53 (1978).
5. P. Pautrot et al., Trans. Am. Nucl. Soc., 20, 202 (1975).
6. V. S. Parbuzin and N. I. Malyavskii, in: Current Problems of Physical Chemistry [in Russian], Vol. 10, Moscow State Univ. (1978), p. 203.
7. P. Gant et al., J. Phys, Chem., 74, 1985 (1970).

POSSIBILITIES AND CONDITIONS FOR VITRIFICATION OF MEDIUM-LEVEL WASTES

V. A. Bel'tyukov, E. V. Brovkova, V. N. Zakharenko,
A. A. Konstantinovich, N. V. Krylova, V. V. Kulichenko,
N. D. Musatov, I. A. Sobolev, and L. M. Khomchik

UDC 621.039.736

The development of methods for solidifying radioactive wastes involves obtaining a material that reliably traps radionuclides and that is highly stable during long-term storage. Even under these conditions, it is natural to strive to remove the product containing the radionuclides as far as possible from human activity. A realistic method for removing the product is storage of solidified radioactive wastes in geological formations, in which it is very desirable to use the smallest possible volumes and areas of the lithosphere.

To solidify medium-level wastes, methods of bituminizing, cementing, vitrification, inclusion in polymers, etc., are being developed. One of the main purposes of solidifying liquid radioactive wastes is to increase the level of safety in temporary storage, transportation, and burial.

Of the materials for which manufacturing processes are currently being developed, vitreous preparations have the best qualities (maximum reduction in volume, lowest rate of leaching of radionuclides, absence of requirements for fire safety in transportation and burial, etc.). In this connection, it is interesting to evaluate the possibility and conditions for vitrification of medium-level wastes. The investigatory and experimental work was performed for a setup using an electrically heated furnace, such as is being developed in the USSR for high-level wastes as well [1].

We studied several accessible minerals as fusing agents (Table 1). Attention was directed primarily toward minerals that do not contain appreciable amonts of alkali-metal compounds, which are one of the basic salt components of medium-level wastes.

The basic investigations were performed with datolite concentrate containing B_2O_3, and fluorite. These components, as is well known, contribute to the decrease in viscosity and melting temperature of the glass mass. It was interesting to also estimate the possibility of using loam, which is the most accessible local raw material in most regions of the country. Medium-level wastes, as a rule, are weakly alkaline or neutral, contain large quantities of alkaline salts and alkali-earth elements, and can contain (except for nitrates) sulfates, fluorides, and chlorides.

We performed the laboratory investigations with liquid waste containing from 260-370 kg/m^3 of $NaNO_3$, 2-8 kg/m^3 of KNO_3, different concentrations of iron compounds (up to 20 kg/m^3), magnesium (up to 35 kg/m^3), calcium (15-60 kg/m^3), chlorides (up to 15 kg/m^3), sulfates (up to 10 kg/m^3), fluorides (up to 10 kg/m^3), etc. These components are typical and are contained both in wastes from nuclear power plants and wastes from fuel reprocessing plants. The chemical stability in water of preparations obtained under laborabory conditions was

TABLE 1. Chemical Composition of Minerals, Mass %

Mineral	CaO	Na_2O	B_2O_3	SiO_2	Al_2O_3	Fe_2O_3	$CaCO_3$	H_2O	CaF_2
Datolite concentrate	28,6	—	17,8	30,7	—	2,6	13,7	6,7	—
Datolite concentrate after calcination	42,0	—	20,0	35,5	—	2,5	—	—	—
Loam	—	5,0	—	70,0	13,0	7,0	—	5,0	—
Quartz sand	—	—	—	99,5	—	—	—	0,5	—
Fluorite	—	—	—	—	—	—	—	0,5	99,5

Translated from Atomnaya Énergiya, Vol. 54, No. 6, pp. 411-413, June, 1983. Original article submitted June 28, 1982.

0038-531X/83/5406-0425$07.50

TABLE 2. Rate of Leaching of Sodium Compounds from Laboratory Specimens of Vitrified Wastes

Composition and ratio of components			Rate of leaching, g/cm² · day		Preparation temperature; viscosity of melts
Oxides of wastes, mass %	mineral, mass %	SiO_2, %	over the first days	after 7 days	
	Datolite concn.				
30	70	—	$5 \cdot 10^{-3}$	$5 \cdot 10^{-4}$	1050° C, 1,3–1,8 Pa · sec
35	65	—	$5 \cdot 10^{-2}$	$1 \cdot 10^{-3}$	
40	60	—	$1 \cdot 10^{-1}$	$5 \cdot 10^{-3}$	
30	30	40	$4 \cdot 10^{-5}$	$7 \cdot 10^{-6}$	1100° C; 2,0–4,5 Pa · sec
30	45	25	$2 \cdot 10^{-5}$	$2 \cdot 10^{-5}$	
40	30	30	$2 \cdot 10^{-4}$	$3 \cdot 10^{-5}$	
	Loam				
41	59	—	$6 \cdot 10^{-5}$	$1 \cdot 10^{-5}$	1200° C; > 10 Pa · sec
52	48	—	$4 \cdot 10^{-4}$	$4 \cdot 10^{-5}$	
	Quartz sand				
42	—	58	$8 \cdot 10^{-5}$	$1 \cdot 10^{-5}$	
62	—	38	$9 \cdot 10^{-4}$	$2 \cdot 10^{-5}$	
	Fluorite				
45	3	52	$7{,}9 \cdot 10^{-5}$	$1{,}5 \cdot 10^{-5}$	1100° C; 5,7 Pa · sec

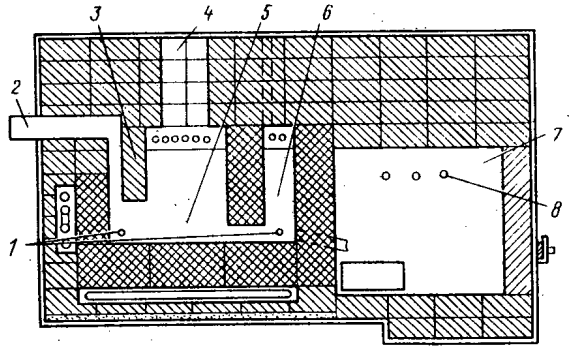

Fig. 1. Arrangement of the furnace for electrical melting: 1) molydenum electrodes; 2) gas conduit; 3) barrier preventing dust entrainment; 4) connecting pipe for load; 5, 6) melting and working zones; 7) unloading chamber; 8) Silit heaters.

estimated from the sodium ion (Table 2). As is evident from Table 2, the rate of leaching from specimens obtained with the use of loam and quartz sand as fusing agents is quite low. However, their melting temperature (> 1200°C) and the viscosity of the melt (> 10 Pa · sec) makes it difficult to obtain these materials in commercial furnaces and to unload them.* In this case it is necessary to introduce additional compounds that contain boron anhydride or calcium fluoride.†

It is most advantageous to use datolite concentrate and fluorite together with quartz sand. As the laboratory investigations demonstrated, when using datolite concentrate, it is possible to obtain a preparation with a very low rate of leaching (see Table 2). For an oxide content in wastes equal to 30 mass %, 25 mass % of quartz sand, and 45 mass % of datolite concentrate at a temperature of 1100°C, the dynamic viscosity of the melt does not exceed 2.2 Pa · sec (22 P). An oxide content in wastes equal to 35–40 mass % and 35–40 mass % SiO_2 in the melt does not greatly change the viscosity: 2.5–3.2 Pa · sec at 1100°C. When

*In melting and clarification of the glass mass in the glass-making industry, the allowable values of viscosity do not exceed 10 Pa·sec (100 P).

†For liquid wastes from nuclear power plants with VVER, which include boric acid, this may not be necessary.

using a fusing agent consisting of fluorite and quartz sand to fix the wastes, the following glass composition is recommended (in mass %): oxides of wastes 45; SiO_2, 50-52; CaF_2, 3-4. The viscosity of the glass melt with this composition at 1100°C is 5.7 Pa · sec.

The amount of fluorine remaining in the glass when using fluorite as the fusing additive is (95 ± 5) mass % (with total fluorine content in the glass equal to 1.6 mass %). When holding the melt obtained with datolite concentrate and quartz sand added as fusing agents and containing 11 g of fluorine per 1 kg of glass mass for 20 h at 1200°C, the fluorine content in the glass did not change.

The low acidity of medium-level wastes makes it difficult to remove the chloride ion in the process of vitrification in the form of volatile hydrogen chloride. In laboratory experiments, up to 80-90 mass % of chlorine (from the starting quantity) is included in the glass mass, while 10-20 mass % is fixed in the vapor–gas phase.

Up to 1 mass % of the sulfate ion relative to its content in the wastes was observed in the vapor–gas flow; the remaining sulfate was included in the glass. However, its distribution in the glass mass is nonuniform, which is indicated by the considerable spread in the results of analysis of the glass in different parts of the glass: The spread increases with increasing sulfate content in the wastes. Apparently, when wastes with the composition studied are vitrified, sulfate is not completely included in the melt and the excess amount of sulfate is mechanically distributed in the glass mass. When wastes containing the sulfate ion in quantities exceeding 10 kg/m^3 are vitrified, a sulfate layer is separated on the surface of the melt.

We performed the experiments on vitrification of wastes using agents based on datolite concentrate on an experimental setup with an electrically heated furnace. Liquid wastes with different degree of dehydration were mixed with the fusing agent, consisting of datolite concentrate and quartz sand in a ratio ensuring that a melt containing 30 mass % of oxides in wastes is obtained. The mixture obtained was inserted into the furnace with the help of a screw conveyor setup (see Fig. 1). The furnace was separated into three zones: melting, working, and unloading. The area of the melting zone was 0.09 m^2 and the area of the working zone was 0.02 m^2. The bottom of the furnace is made of the DVD-11 ceramic with high aluminum-oxide content, the walls were made of ShA-3 fireclay, and the bottom and walls of the furnace are water cooled. The charge is introduced into the furnace with the help of the screw conveyor setup through water-cooled connecting pipes. To prevent dust entrainment, the charge loading zone is separated from the gas line by a barrier. Power is introduced by passing alternating current through two horizontally positioned molybdenum electrodes with diameter 18 mm. The distance between the electrodes is 400 mm.

The glass mass is poured through the pouring connecting pipe into a special chamber. To prevent cooling of the stream of glass mass, the temperature in the unloading zone was maintained at 800-900°C with the help of Silit heaters. The vapor–gas mixture enters from the furnace through the gas conduit into a gas scrubbing system, consisting of a bubbler-condenser, adsorber for trapping nitrogen oxides, and filters for coarse and fine cleaning.

We performed two series of experiments with liquid wastes on this setup. The solution capacity was $6 \cdot 10^{-3}$ m^3/h and was chosen taking into account the optimum ratio of the area of the melting zone of the furnace and the volume of the solution, determined when developing the vitrification process for high-level wastes [1]. In the second series of experiments we introduced molasses into the solution. The interaction of molasses with the nitrate ions during calcination of the solution leads to the formation of a loose foam on the surface of the glass melt, which excludes the formation of a dense crust of calcinated product in the furnace and decreases the amount of radionuclides carried away with the vapor–gas phase [2]. We performed the experiments on wastes with the same composition used to check the process of bituminization, included in the design of nuclear power plants.

The results of the experiments are presented below:

Salt concentration in wastes, kg/m^3	450	450*	930
Specific β activity of wastes, Bq/m^3	$1.8 \cdot 10^9$	$1.8 \cdot 10^9$	$3.7 \cdot 10^9$

Capacity:			
with respect to liquid wastes, 10^{-3} m^3/h	6 ±0.6	6 ±0.6	10 ±1
with respect to glass, $kg/(m^2 \cdot h)$	34 ±3	34 ±3	85 ±8
Temperature, °C:			
glass mass	1100-1150	1150-1200	1100-1150
outgoing gases	130	130	200-220
Consumption of electricity, kW · h	7.2	7.0	13.2
Matter carried out of the furnace, %†:			
solid phase	1.0	0.4	0.9
^{90}Sr	0.5	0.3	0.3
^{137}Cs	4.6	2.7	2.8
sum of α emitters	0.6	0.6	0.6
boron anhydride	7.5	4.2	4.7

The higher removal of ^{137}Cs and B_2O_3 from the furnace compared with the removal of ^{90}Sr and of the solid phase is explained by the high vapor pressure of compounds of these components. Boron leaves the furnace mainly in the form of alkaline borates and metaboric acid, whose evaporation increases in the presence of water [3]. The decrease in matter carried away with introduction of molasses is related with the filtering action of the foamlike product forming on the surface of the melt.

The glass-mass capacity of the furnace can be increased by initially decreasing the water content of the wastes. A concentrate obtained by concentrating liquid wastes in a drum dryer up to a salt content of 930 kg/m^2 was used in these experiments. The rate at which the wastes are introduced into the furnace was chosen according to the conditions for performing the process when the surface of the melt is completely covered by a layer of calcinated product. Removal of material was further reduced by reprocessing the additionally concentrated wastes and the glass-mass capacity of the furnace increased.

The volume of solidified wastes obtained as a result of vitrifying 1 m^3 of liquid wastes is 0.2-0.3 m^3, which is a factor of 3.7 smaller than the volume obtained by including the wastes in bitumen and polymers and almost ten times smaller than the volume of the cement block obtained with the same wastes. The rate of leaching out of the least strongly bound radionuclide ^{137}Cs is $(2-3) \cdot 10^{-6}$ $g/(cm^2$ day), which is two orders of magnitude lower than the rate of leaching out of a block of bitumen and four orders of magnitude lower than the rate of leaching out of cement. Another advantage is the elimination of contamination of water and soil by nitrates as a result of the absence of these ions in the glass block. Because there is no danger of fire, the transportation and burial processes are simplified, although compared to bituminization and cementing, the apparatus for the solidification process is more complicated, which is related with the necessity of using high temperatures.

In order to introduce the vitrification method at nuclear power plants, additional work must be performed on improving the apparatus, and a number of problems involving repeated use of the condensate must be solved.

LITERATURE CITED

1. A. A. Konstantinovich et al., in: Proceedings of the Fourth Scientific-Technical Conference SEV "Research on Making Liquid, Solid, and Gaseous Radioactive Wastes Harmless and Deactivation of Contaminated Surfaces," Atomizdat, Moscow (1978), No. 2, p. 110.
2. A. A. Konstantinovich et al., ibid., p. 90.
3. A. A. Appen, Chemistry of Glass [in Russian], Khimiya, Moscow (1974), p. 229.

*Addition of molasses (100 kg/m^3).
†Average data from several experiments are presented.

CALCULATION OF A COMPLEX GRID WITH CLUSTERS IN THE SINGLE-GROUP P_3 APPROXIMATION

V. E. Raevskaya and B. Z. Torlin

UDC 621.039.51

In the Galanin—Fainberg theory, the neutron field is described by the superposition of the field of individual assemblies placed at grid points of a homogeneous reactor. The diffusional approximation, in which the assemblies are replaced by individually calculated effective boundary conditions at their surface, is more developed [1]. In [2], the basic idea of heterogeneous theory — the superposition principle — is extended to the P_3 approximation. In this case the neutron field is calculated simultaneously in the assemblies and in the interchannel moderator. In the programs realized [2, 3], the grid was regarded as not being tight and the "intrinsic" field of the assemblies as azimuthally isotropic (the monopole approximation). Subsequently, the numerical method was refined [4, 5] as a result of the use of matrix fitting to calculate the neutron field inside the assemblies. This guaranteed numerical stability of the method for any assemblies both with black and with transparent layers, and provided a series of additional conveniences in calculations. As shown in [4], this procedure reduces to calculation of the matrix $\hat{\gamma}$ and the vector D relating the three-component "flux" φ and the current j of neutrons at each concentric boundary of the multilayer assembly by the boundary condition

$$\mathbf{j}=\hat{\gamma}\varphi+\mathbf{D}. \tag{1}$$

Using recurrence relations, the matrix $\hat{\gamma}$ and vector D are calculated successively from the center to the external surface of the assembly. After determining $\hat{\gamma}$ and D at the surfaces of the assemblies, the neutron fluxes there are calculated by the scheme outlined in [4, 5], similar in general outline to the scheme of the analogous calculation of heterogeneous grids in the diffusional approximation. These principles of the construction of solutions in grids with multiring assemblies are also valid for assemblies containing bundles of cylindrical (and even multiring) fuel elements immersed in coolant, i.e., clusters.

The neutron field of the cluster is represented as the superposition of the fields of the individual rods. Then, following [2, 4], the following expressions are obtained in the monopole approximation at the surface of the k-th rod ρ_k:

$$\varphi(\rho_k)=\sum_n \hat{F}_n^{(1)}(\rho_k)\,\mathbf{A}_n+\hat{f}^{(1)}(\rho_k)\,\mathbf{B}+\mathbf{C}^{(1)}(\rho_k); \tag{2a}$$

$$\mathbf{j}(\rho_k)=\sum_n \hat{F}_n^{(2)}(\rho_k)\,\mathbf{A}_n+\hat{f}^{(2)}(\rho_k)\,\mathbf{B}+\mathbf{C}^{(2)}(\rho_k). \tag{2b}$$

Here A, B, and C are three-component vectors; $\hat{F}$, $\hat{f}$, 3×3 matrices; and C, source vectors described in [4]; A are the amplitudes of the "intrinsic" fields of the rods and, for equivalent rods (with identical "intrinsic" fields), may be taken outside the summation sign. Then the summation is taken not over all the rods but only over all the monequivalent elements. The rules for the formation of the matrices $\hat{F}$ and the calculation of their elements were described in sufficient detail in [5].

The appearance of the second terms on the right-hand side of Eq. (2) is relatively new here. These are associated with the finiteness of the cluster dimensions and are absent in infinite grids. For matrix $\hat{f}$, the matrix elements $f_{\eta\nu}^{\delta}(\rho_k)=c_{\eta\nu}I_m\left(\frac{\alpha_\nu\rho_k}{l}\right)I_0\left(\frac{\alpha_\nu r_k}{l}\right)$. Here r_k is the distance from the cluster axis to the axis of the k-th rod. The coefficients $c_{\eta\nu}$ are

Translated from Atomnaya Énergiya, Vol. 54, No. 6, pp. 415-417, June, 1983. Original article submitted April 19, 1982.

0038-531X/83/5406-0429$07.50

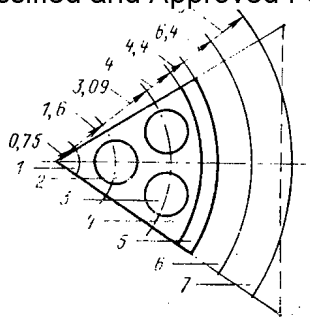

Fig. 1. Symmetry element (one sixth) of the RBMK-reactor channel: 1) zirconium rod; 2, 3) elements; 4) vapor–water mixture; 5) zirconium tube; 6, 7) graphite.

given in [2, 3]. The relation between the number of rows n and the index of the modified Bessel function I_m is established by means of the following relations: If n = 1, 2, and 3, then m = β − 1 and β + 1, respectively, while

$\alpha_\nu^2 = \frac{35}{18} a \left(1 \mp \sqrt{1 - \frac{108\varepsilon}{35} \frac{1-\mu+\varepsilon\mu}{a^2}}\right)$ for ν = 1 and 2, $\alpha_3^2 = 7$; $\varepsilon = l/l_a$ (where l and l_a are the total interaction length and the absorption length of neutrons in the coolant, respectively); μ is the mean cosine of the angle of neutron scattering; $a = 1 + \varepsilon \left[\frac{11}{7} - \frac{27}{35}\mu(1-\varepsilon)\right]$.

From symmetry considerations, equivalent elements must be at the same distance from the cluster axis, be congruent, and have identical physical properties. Then the k-th group of M_k equivalent elements may be any rod at a distance r_k from the cluster axis with an external radius ρ_k, boundary matrix $\hat{\gamma}(\rho_k)$, and vector $D(\rho_k)$.

The vectors $\varphi(\rho_k)$ of these representations of all N equivalent groups are combined into the vector $\varphi_{cl} = \mathrm{col}[\varphi(\rho_1), \ldots, \varphi(\rho_N)]$, the vectors $j(\rho_k)$ into the vector $j_{cl} = \mathrm{col}[j(\rho_1), \ldots, j(\rho_N)]$, the vectors $D(\rho_k)$ into the vector $D_{cl} = \mathrm{col}[D(\rho_1), \ldots, D(\rho_N)]$, and the vectors A_k and C_k into the vectors $A_{cl} = \mathrm{col}(A_1, \ldots, A_N)$ and $C_{cl}^{(\beta)} = \mathrm{col}[C^{(\beta)}(\rho_1), \ldots C^{(\beta)}(\rho_N)]$. These new vectors are of dimensionality 3N.

A series of new matrices are also formed: diagonally cellular matrices $\hat{\gamma}_{cl} = \{\hat{\gamma}(\rho_k)\delta_{kn}\}$ and square matrices $\hat{F}_{cl}^{(\beta)} = \{\hat{F}_n^{(\beta)}(\rho_k)\} = \{\hat{F}_{cl}^{(\beta)}\}_{kn}$ $(k = 1, \ldots, N;\ n = 1, \ldots, N)$ of dimensionality 3N × 3N, and also rectangular (vertical) matrices $\hat{f}_{cl}^{(\beta)} = \{f^{(\beta)}(\rho_k)\}$ of dimensionality 3N × 3. In the new notation, Eqs. (1) and (2) take the following form for all k:

$$j_{cl} = \hat{\gamma}_{cl}\varphi_{cl} + D_{cl}; \tag{3a}$$

$$\varphi_{cl} = \hat{F}_{cl}^{(1)} A_{cl} + \hat{f}_{cl}^{(1)} B + C_{cl}^{(1)}; \tag{3b}$$

$$j_{cl} = \hat{F}_{cl}^{(2)} A_{cl} + \hat{f}_{cl}^{(2)} B + C_{cl}^{(2)}. \tag{3c}$$

Using the theorem of addition of cylindrical functions, relations similar to Eq. (2) may also be obtained for the external surface of the cluster R_{cl}:

$$\varphi(R_{cl}) = \hat{F}^{(1)}(R_{cl}) A_{cl} + \hat{I}^{(1)}(R_{cl}) B + C^{(1)}(R_{cl}); \tag{4a}$$

$$j(R_{cl}) = \hat{F}^{(2)}(R_{cl}) A_{cl} + \hat{I}^{(2)}(R_{cl}) B + C^{(2)}(R_{cl}). \tag{4b}$$

The square matrices $\hat{I}$ of dimensionality 3 × 3 here are as in [4], while the rectangular matrices (horizontal) of dimensions 3 × 3N are formed as $\hat{F}^{(\beta)}(R_{cl}) = \{\hat{F}_n^{(\beta)}(R_{cl})\}$ from the matrices $F_n(R_{cl})$ of dimensions 3 × 3 with matrix elements equal to $c_{\nu\nu} M_n K_m \left(\frac{\alpha_\nu R_{cl}}{l}\right) I_0 \left(\frac{\alpha_\nu r_n}{l}\right)$, where K_m are modified Hankel functions of m-th order.

Equations (3) and (4) are similar to the analogous expressions from [4], differing only in dimensionality. Therfore, following [4],

$$j(R_{cl}) = \hat{\gamma}(R_{cl})\varphi(R_{cl}) + D(R_{cl}); \tag{5a}$$

TABLE 1. Mean in Neutron Fluxes in the Channel of an RBMK Reactor with a Grid Step of 15.95 cm*

Zone number	Material	ρ_k, cm	$\bar{\Phi}_{P_3}$	$\bar{\Phi}^0_{G_3}$	$\frac{\bar{\Phi}_{P_3}-\bar{\Phi}^0_{G_3}}{\bar{\Phi}^0_{G_3}}$, %	$\bar{\Phi}^1_{G_3}$	$\frac{\bar{\Phi}_{P_3}-\bar{\Phi}^1_{G_3}}{\bar{\Phi}^1_{G_3}}$, %
			When $\rho_{H_2O}=1$				
1	Zr	0,75	0,0883	0,0885	—0,2	0,1033	—14,6
2	UO_2	1,6	0,0787	0,0777	1,3	0,0895	—12,0
3	UO_2	3,09	0,1247	0,1226	1,7	0,1176	6,0
4	H_2O	4	0,1480	0,1495	—1,0	0,1442	2,6
5	Zr	4,4	0,2267	0,2259	0,3	0,1988	14,0
6	C	6,4	0,2407	0,2400	0,3	0,2129	13,0
7	C	9	0,2550	0,2519	1,2	0,2248	13,4
			When $\rho_{H_2O}=0,6$				
1	Zr	0,75	0,0885	0,0899	—1,5	0,1019	—13,2
2	UO_2	1,6	0,0833	0,0825	1,0	0,0910	—9,3
3	UO_2	3,09	0,1268	0,1245	1,8	0,1208	5,0
4	H_2O	4	0,1438	0,1473	—2,3	0,1442	—0,3
5	Zr	4,4	0,2131	0,2140	—0,4	0,1965	8,4
6	C	6,4	0,2334	0,2343	—0,4	0,2167	7,7
7	C	9	0,2538	0,2512	1,1	0,2336	8,7
			When $\rho_{H_2O}=0,2$				
1	Zr	0,75	0,0976	0,1066	—8,4	0,1017	—4
2	UO_2	1,6	0,0944	0,0952	—0,8	0,0917	3,0
3	UO_2	3,09	0,1256	0,1226	2,5	0,1241	1,2
4	H_2O	4	0,1341	0,1413	—5,1	0,1425	—5,9
5	Zr	4,4	0,1824	0,1879	—2,9	0,1946	—6,3
6	C	6,4	0,2180	0,2230	—2,2	0,2297	—5,1
7	C	9	0,2532	0,2518	5,7	0,2585	—2,0

*Here and in Table 4, the normalization of the flux is arbitrary.

TABLE 2. Initial Data

Material	Σ_{tot}, cm^{-1}	Σ_a, cm^{-1}	q, cm^{-3}
Zirconium	0,3475	0,0075	0,00755
Graphite	0,4000	0,0003	0,0636
Water ($\rho_{H_2O}=1$)	2,3900	0,0170	1,3660
Fuel	0,6708	0,3233	0

$$\varphi_{cl}=\hat{E}_{cl}\varphi(R_{cl})+\sigma_{cl}. \tag{5b}$$

where

$$\hat{\gamma}(R_{cl})=\hat{L}^{(2)}[\hat{L}^{(1)}]^{-1}; \tag{6}$$

$$\hat{E}_{cl}=\hat{L}_{cl}[\hat{L}^{(1)}]^{-1}; \tag{7}$$

$$\mathbf{D}(R_{cl})=[\hat{F}^{(2)}(R_{cl})-\hat{\gamma}(R_{cl})\hat{F}^{(1)}(R_{cl})]\hat{F}\mathbf{d}-$$
$$-\hat{\gamma}(R_{cl})\mathbf{C}^{(1)}(R_{cl})+\mathbf{C}^{(2)}(R_{cl}); \tag{8}$$

$$\sigma_{cl}=[\hat{F}^{(1)}_{cl}-\hat{E}_{cl}\hat{F}^{(1)}(R_{cl})]\hat{F}\mathbf{d}-\hat{E}_{cl}\mathbf{C}^{(1)}(R_{cl})+\mathbf{C}^{(1)}_{cl}; \tag{9}$$

$$\hat{L}^{(\beta)}=\hat{f}^{(\beta)}(R_{cl})+\hat{F}^{(\beta)}(R_{cl})\hat{F}\hat{f};$$

$$\hat{L}_{cl}=\hat{f}^{(1)}_{cl}+\hat{F}^{(1)}_{cl}\hat{F}\hat{f};$$

$$\hat{F}=[\hat{F}^{(2)}_{cl}-\hat{\gamma}_{cl}\hat{F}^{(1)}_{cl}]^{-1};$$

$$\hat{f}=\hat{\gamma}_{cl}\hat{f}^{(1)}_{cl}-\hat{f}^{(2)}_{cl};$$

$$\mathbf{d}=\hat{\gamma}_{cl}\mathbf{C}^{(1)}_{cl}-\mathbf{C}^{(2)}_{cl}+\mathbf{D}_{cl}$$

TABLE 3. Use Coefficients of Thermal Neutrons in the Channel of an RBMK Reactor

ρ_{H_2O}	θ_{P_3}	$\theta_{G_3^0}$	$\theta_{G_3^1}$	$\frac{\theta_{P_3}-\theta_{G_3^0}}{\theta_{G_3^0}}$, %	$\frac{\theta_{P_3}-\theta_{G_3^1}}{\theta_{G_3^1}}$, %	$\frac{\theta_{G_3^0}-\theta_{G_3^1}}{\theta_{G_3^1}}$, %
0	0,9114	0,9098	0,9150	0,18	—0,39	—0,57
0,6	0,9358	0,9340	0,9370	0,18	—0,13	—0,31
0,2	0,9606	0,9589	0,9580	0,18	0,26	0,08
$\theta_{\rho=0,2}-\theta_{\rho=1}$	0,0492	0,0491	0,0430	—	—	—
$\theta_{\rho=0,6}-\theta_{\rho=1}$	0,0244	0,0242	0,0220	—	—	—

TABLE 4. Neutron Fluxes in Zones of Polycell Assemblies

Zone number	Material	Assembly number								
		1	2	3	1	2	3	1	2	3
		ρ_{H_2O}			ρ_{H_2O}			ρ_{H_2O}		
		1,0	0,6	0,2	1,0	0,6	0,6	0,2	0,6	0,6
1	Zr	3,994	3,579	4,431	4,029	3,697	3,677	4,291	3,501	3,527
2	UO_2	3,755	3,611	4,379	3,811	3,754	3,730	4,239	3,516	3,548
3	UO_2	7,244	6,683	6,218	7,506	7,057	6,995	6,011	6,436	6,520
4	H_2O	8,518	7,477	6,584	8,819	7,887	7,818	6,366	7,206	7,298
5	Zr	14,658	12,477	9,459	15,332	13,267	13,136	9,137	11,954	12,131

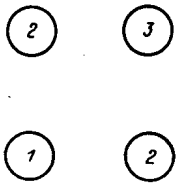

Fig. 2. Cartogram of the polycell in the calculation.

Thus, the cluster is characterized by the boundary conditions in Eqs. (5a), (6), and (8) at its external boundary, and further calculation of the assembly and the whole grid may be performed by the scheme described in [4]. On the basis of the foregoing, the CLUST program is written [6]; it is similar to programs already described. By its use, however, calculations may be made in the single-group P_3 approximation for both quadratic and hexagonal polycells containing not only multiring assemblies, but also assemblies including bundles of multiring fuel elements.

The cross section of part of the channel of an RBMK reactor is shown in Fig. 1. The results of calculating these channels in a homogeneous square grid by the CLUST program and in cylindrical geometry by the PRAKTINEK program [7] on the basis of the G_N^p method (where N is the number of spherical harmonics used and p is the number of azimuthal harmonics used) of surface pseudosources are given in Table 1. The initial data for this calculation are given in Table 2. Table 3 gives values of the thermal-neutron use coefficients θ. It follows from the given data that monopolar P_3 and G_3^0 approximation lead to very similar results. The neutron fluxes calculated in the more accurate* G_3^1 approximations differ markedly from these results (the maximum discrepancy reaches almost 15% at the center of the cluster with a water density $\rho_{H_2} = 1$); the difference in the value of θ is small. Whereas the present calculation has the aim of comparing new results with those already existing and being able

*As shown in [7], the neutron fluxes calculated by the Monte Carlo and G_3^1 methods coincide, with a statistical error of $\leqslant 2\%$.

to establish the efficiency of the program and sufficient accuracy of the approximation, future investigations should demonstrate the programs in calculations of polycells.

A cartogram of the assembly positions (with equivalence numbers) in the polycell is shown in Fig. 2, results of the calculation of which by the CLUST program are given in Table 4. The assembly geometry is as in the preceding example. The grid step is 25 cm. As follows from Table 4, the neutron flux increases in assemblies with an increased coolant density on account of increase in the volume density of sources. This effect should facilitate an increase in the vapor content in the polycell. The fuel elements are regarded as single-zone only because the constants of the preceding calculation are used. The CLUST program allows assemblies and rods with up to 30 annular zones to be calculated. The possible number of nonequivalent rods is up to 10, and the maximum number of nonequivalent assemblies in the polycell is 10. The calculation time for a double grid is 20-30 sec, depending on the number of zones in the assembly. The maximum calculation time of a variant is ∿4 min. The program is written in FORTRAN for a BÉSM-6 computer.

It remains to thank A. D. Galanin and B. P. Kochurov for discussion of the work and assistance in choosing examples.

LITERATURE CITED

1. A. D. Gaalnin, Theory of a Heterogeenous Reactor [in Russian], Atomizdat, Moscow (1971).
2. A. D. Galanin and B. Z. Torlin, At. Energ., 36, No. 2, 125 (1974).
3. V. E. Raevskaya and B. Z. Torlin, Preprint ITEF, No. 60 (1977).
4. V. E. Raevskaya and B. Z. Torlin, At. Energy., 49, No. 5, 310 (1980).
5. V. E. Raevskaya and B. Z. Torlin, Preprint ITEF No. 127 (1980).
6. V. E. Raevskaya, Preprint ITEF No. 22, (1982).
7. N. V. Sultanov, Preprint IAE No. 3005 (1978).

DETERMINATION OF THE CROSS SECTION OF THE REACTION $^{27}Al(n, p)^{27}Mg$ WITH NEUTRONS OF ENERGY 14.8 MeV

V. T. Shchebolev, N. N. Moiseev, and Z. A. Ramendik

UDC 539.172.4

The value of the (n, p)-reaction cross section in aluminum is widely used in calculations of the structures of nuclear physics facilities as a reference value when measuring the cross sections in other elements, and also when measuring the neutron flux density on accelerators. In particular, in Great Britain foils of aluminum are certified, taking account of the value of the activation cross section as a secondary standard of the unit of neutron flux density [1]. However, as the published data differ strongly (up to 20%), the problem of the exact measurement of the cross section σ of the reaction $^{27}Al(n, p)^{27}Mg$ is urgent.

In the present paper, samples of specially pure aluminum are used in the form of disks with diameter 30 mm adn with a thickness from 0.5 to 1.0 mm. The number of nuclei in the specimene was determined from the results of accurate weighing and chemical and mass-spectrometric analyses.

Irradiation was carried out in the field formed by a neutron generator as the result of excitation of the reaction $T(d, n)^4He$. The distance (6-12 cm) between the sample and the center of the tritium target was measured with an error of ≤ 0.02 mm, and its azimuthal position relative to the direction of the deuteron beam was measured with an error of 0.0006 rad. The neutron energy was $14.8^{+0}_{-0}{}^{.1}_{.2}$ MeV. The neutron flux density was determined by several independent methods [2] with an error not exceeding 1% (with confidence coefficient of $P = 0.99$). Irradiation was continued for 30 to 60 min, and 10 min after completerion the induced activity was measured by the absolute β-γ-coincidence method and on a γ-scintillation spectrometer, the efficiency of which was determined beforehand with respect to standard sources from the OSGI collection. In the latter case, certain OSGI sources (in particular, ^{54}Mn and ^{65}Zn) were certified with an error of 1.0-1.5% for $P = 0.99$. A standard program was used for processing the spectral distributions and for calculating the area under the photopeaks. A UNO-4096 analyzer was used for the measurements. The effects of the neutron flux density variation over the thickness of the sample with time, during prolonged irradiation, geometrical factor, etc., were taken into account.

The sources of the component errors and estimates of their values, taking account of the weight factors, are given in Table 1 (S_0 is the mean-square deviation, θ_0 is the unincluded systematic error).

The results of the experimental determination of the cross section of $^{27}Al(n, p)^{27}Mg$, obatained in the present paper, are as follows ($1\ b = 10^{-28}\ m^2$): $\sigma_1 = 68.0$ mb; $\sigma_{01} = 1.6\%$ — β-γ-coincidence method; $\sigma_2 = 68.5$ mb; $\delta_{02} = 2.1\%$ — γ-spectrometer method. The mean-square value of $\sigma(n, p) = (68.2 + 0.9)$ mb is taken as the final result.

Table 2 gives the data of some original papers on the experimental determination of the cross section of the (n, p) reaction on aluminum, with errors not exceeding 10%, for a range of neutron energies of 14.6-14.9 MeV.

According to the criteria of adequacy of the group of data and their membership to one and the same general set, the value from [4] must be excluded from further consideration. The average value of the cross section obtained without taking account of the measurement errors is equal to (71.0 ± 1.1) mb, and in this case S_{01} of the series of measurements (column

Translated from Atomaya Énergiya, Vol. 54, No. 6, pp. 417-419, June, 1983. Original article submitted June 2, 1982.

 0038-531X/83/5406-0434$07.50

TABLE 1. Estimates of the Errors in the Determinaton of the Cross Section

Source of error	Method of measurement			
	β−γ coincidence		γ spectrometer	
	S_0, %	θ_0, %	S_0, %	θ_0, %
Determination of neutron flux density	—	0,6	—	0,6
Determination of number of nuclei in sample	—	0,05	—	0,05
Decay constant	—	0,2	—	0,1
Measurement of time intervals	—	0,1	—	0,1
Activity measurement	0,2	0,8	—	—
Determination of area under photopeaks	—	—	0,3	0,5
Determination of γ-spectrometer efficiency y	—	—	—	1,0
Total	0,2	1,4	0,3	1,8
Total relative error δ_0	1,6		2,1	

TABLE 2. Cross Section of the $^{27}Al(n, p)-^{27}Mg$ Reaction

Proton energy, MeV	σ (E), mb	Literature	Scaled cross section, mb
14,60	74,47±4,2	[3], 1973	72,95±4,2
14,65±0,10	67,3±2,0	[4], 1978	66,16±2,0
14,67±0,09	78,0±5,5	[5], 1968	77,01±5,5
14,70±0,15	66,0±2,0	[6], 1964	65,24±2,0
14,70±0,15	73,0±2,0	[7], 1970	72,24±2,0
14,75±0,25	68,0±5,0	[8], 1960	67,62±5,0
14,78±0,10	68,0±2,3	[1], 1973	67,85±2,3
14,8±0,9	54,0±5,0	[9], 1959	54,0±5,0
14,80±0,20	73,0±5,0	[10], 1970	73,0±5,0
14,80	75,0±6,0	[11], 1971	75,0±6,0
14,8	70,58±3,4	[12], 1974	70,58±3,4
14,9	71±5	[13], 1978	71,76±5,0
$14,8^{+0,1}_{-0,2}$	68,2±0,9	Present paper	68,2±0,9

2, Table 2) amounts to 3.5 mb; the average value without taking our value into account is equal to (71.3 ±1.1) mb; $S_{02} = 3.5$ mb, and the estimate of S_{03} by difference amounts to 3.5 mb.

The estimates given above for the cross section values were obtained without taking account of the difference in the neutron energies for the range 14.6-14.9 MeV. The values, scaled to an energy of 14.8 MeV, are given in column 4 of Table 2, using the gradient of the excitation curve of the reaction equal to −7.6 mb/MeV [14] for the stated energy range. In this case the similar estimates of the value and errors amount to: arithmetic mean (70.6 ±1.1) mb, $S_{01} = 3.6$ mb; arithmetic mean without taking our result into account (70.8 ±1.1) mb, $S_{02} = 3.6$ mb; estimate of S_{03} by difference equal to 3.5 mb. The mean weighted value (column 4, Table 2) amounts to (68.6 ±0.6) mb, and without taking our result into consideration it is (68.9 ±0.9) mb. Thus, the most reliable value from the data given should be assumed to be the mean weighted value of σ = (68.6 ±0.6) mb.

When determining the (n, p) cross section by the γ-spectrometry method, the area under the ^{27}Mg photopeak was obtained as the sum of the areas under the photopeaks of the 0.842 and 1.010 MeV lines, taking into account the variation of efficiency of the spectrometer in this energy range. The efficiency for the energies 0.835 and 1.115 MeV was determined with high accuracy by ^{54}Mn and ^{65}Zn γ-quanta sources. Comparison of the photopeaks corresponding to the 0.842 and 1.010 MeV lines of ^{27}Mg allowed the quantum yield of this radionuclide to

be obtained — equal to 69.8 and 30.2% respectively. The error of the determination of the relative quantum yield amounted to 2.3%. The values obtained for the probability of decay of ^{27}Mg by two channels coincides quite well with the data given in [15] — 71.5 and 28.5%; however, they disagree with the data of [6] — 58 and 42%.

LITERATURE CITED

1. J. Robertson et al., J. Nucl. Energy, 27, No. 3, 139 (1973).
2. V. T. Shchebolev and Z. A. Ramendik, in: Neutron Physics. Data of the Fifth All-Union Conference [in Russian], Central Scientific-Reasearch Institute-Atominform, Moscow, Part 4 (1980), p. 270.
3. Report IER-1464, 12 (1973).
4. T. Ryves et al., J. Phys, G: Nucl. Phys., 4, No. 11, 1783 (1978).
5. J. Cazzocrea et al, Nuovo Cimento, 54, 538 (1968).
6. G. Bonazzola et al., Nucl. Phys., 51, 337 (1964).
7. W. Shante, Thesis Vienna University, Vienna (1970).
8. C. Mani et al., Nucl. Phys., 19, 535 (1960).
9. A. Poularicas and R. Fink, Phys. Rev., 115, 989 (1959).
10. L. Husain et al., Phys. Rev., C1, 1233 (1970).
11. G. Salaite, Nucl. Phys., A170, 193 (1971).
12. T. Navoddot et al., Inorg. Nucl. Chem., 36, No. 5, 953 (1974).
13. V. I. Melent'ev and V. V. Ovechkin, At. Energ., 44, No. 2, 171 (1978).
14. E. A. Borisov et al., in: Metrology of Neutron Measurements on Nuclear-Physics Facilities [in Russian], Central Scientific-Research Institute-Atominform, Moscow, Vol. 1 (1976), p. 194.
15. N. G. Gusev and P. P. Dmitriev, Quantum Emission of Radioactive Nuclides (Handbook) [in Russian], Atomizdat, Moscow (1977).
16. B. S. Dzhelepov et al., Decay Schemes of Radioactive Nuclei [in Russian], Nauka, Moscow (1966).

ESTIMATE OF THE INTERCRYSTALLINE ADSORPTION OF HELIUM IN NICKEL

É. U. Grinik and V. S. Karasev

UDC 621.039.531:539.67

The buildup of helium at grain boundaries promotes high-temperature radiation embrittlement of materials [1] and affects the grain-boundary relaxation [2]. For the experimental determination of the very slight changes of concentration of impurities at the grain boundaries, it is advantageous to use the method of internal friction. The height and temperature of the grain-boundary maximum varies in proportion to the change of concentration of impurity and these variations cease with the adsorption saturation of the grain boundaries by impurities without phase separation [3].

The binding energy of the impurity with the grain boundaries F is determined by the relation:

$$F = -kT_n \ln (C_{gr}/C), \tag{1}$$

where k is Boltzmann's constant; T_n is the temperature corresponding to the grain-boundary maximum of internal friction at the instant of attaining saturation; C and C_{gr} are the concentration of impurities in the material and in the adsorption zone of the grain boundaries.

The concentration of impurities in the adsorption zone is expressed by the degree of filling, i.e., by the ratio of the number of impurity atoms to the number of adsorption centers of the given impurity [3]. In the case of saturation, when all adsorption centers are filled, $C_{gr} = 1$ [3], and relation (1) assumes the form

$$F = -kT_n \ln (1/C). \tag{2}$$

Relation (2) enables F to be determined on the basis of the experimental data concerning the temperature T_n and the calculated values of the helium concentration C for a duration of irradiation corresponding to the attainment of steady values of the temperature and height of the internal friction peaks.

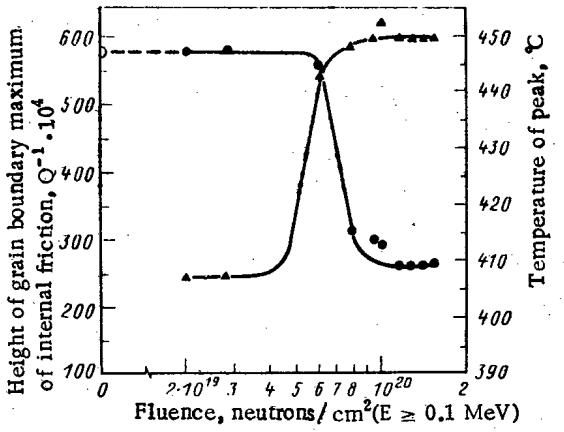

Fig. 1. Dependence of the variation of height (●) and temperature (▲) of the grain-boundary internal-friction maximum of nickel during reactor irradiation on the neutron fluence; ○) height of peak before irradiation.

Translated from Atomnaya Énergiya, Vol. 54, No. 6, pp. 419-420, June, 1983. Original article submitted June 22, 1982.

0038-531X/83/5406-0437$07.50

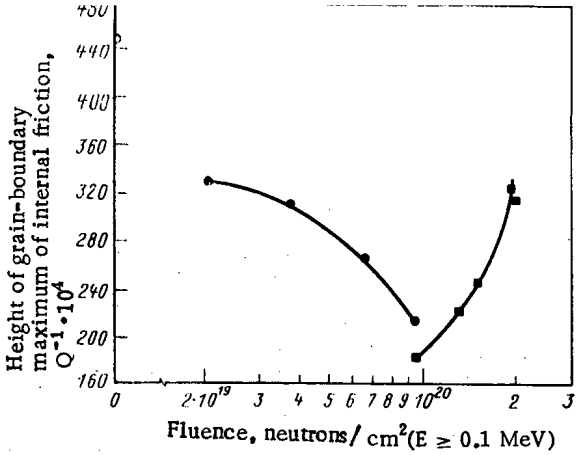

Fig. 2. Dependence of the variation of height of the principal (●) and impurity (■) grain-boundary internal-friction maxima of the alloy Ni—^{10}B during irradiation on the neutron fluence.

Experiments were conducted on specimens of polycrystalline nickel (grain size ∿50 μm) from electron-beam smelting, with purity 99.99%, by the procedure described previously in [4]. The diameter and length of the specimens was 0.8 and 70 mm. After annealing for 1 h at a temperature of 700°C in a vacuum of ∿13 mPa, the initial temperature dependence of the internal friction was determined, representing the exponentially increasing background component, on which is superimposed the grain-boundary maximum for a temperature of 450°C. The frequency of the torsional vibrations amounted to 5-7 Hz, and the amplitude of the relative deformation of the surface of the specimen was maintained equal to $3 \cdot 10^{-5}$. The measurement ampul, with this specimen, was loaded into the material behavior channel of the VVR-M reactor in the Institute of Nuclear Research, Academy of Sciences of the Ukrainian SSR. The irradiation temperature (350°C) was maintained constant but was raised briefly during the measurements to 650°C; the fast (E ≥ 0.1 MeV) neutron flux density amounted to $\sim 10^{14}$ neutrons/($cm^2 \cdot sec$), and the thermal neutron flux density was $\sim 5 \cdot 10^{13}$ neutrons/($cm^2 \cdot sec$).

During irradiation the height of the grain-boundary internal-friction maximum decreased in proportion with increase of the neutron fluence, but the temperature corresponding to this maximum, on the contrary, increased (Fig. 1), and in both cases saturation was attained with an identical fast neutron fluence ($\sim 1.2 \cdot 10^{20}$ neutrons/$cm^2 \cdot sec$). This behavior of the parameters of internal friction is characteristic for the adsorption saturation of the grain boundaries by impurities.

The effect revealed should be related to the saturation of the grain boundaries with helium, formed as the result of the (n, α) reaction. For confirmation, experiments were carried out to measure the internal friction in the case of the irradiation of platinum and specimens of nickel of the same batch but alloyed with 0.007 mass % of ^{10}B, which is disposed mainly over the grain boundaries. For the samples of platinum, in which no (n,α)-reactions occur, no changes of the grain-boundary internal-friction maximum were detected, for a fast neutron fluence of $\leq 5 \cdot 10^2$ [sic] neutrons/cm^2. In samples of Ni—^{10}B, for which the cross section of the $^{10}B(n, \alpha)^7Li$ reaction by thermal neutrons amounts to 3838 b [5] (1 b = 10^{-28} m^2), the height of the principal grain-boundary internal-friction maximum first of all decreased in proportion with the increase of the neutron fluence, as in the case of the sample of pure nickel (Fig. 2), and then, with a fast neutron fluence of $\sim 10^{20}$ neutrons/cm^2, a second internal friction peak appeared, due to the presence of lithium, the height of which increased with increase of the neutron fluence. The experiments confirmed that the change of parameters of the grain-boundary internal-friction maximum for pure nickel actually is due to saturation of the grain boundaries by helium.

A calculation of the helium formation, taking account of the isotopic composition of nickel and of the VVR-M neutron spectrum, and also of the secondary nuclear reaction in ^{59}Ni, shows that with a fast neutron fluence of $1.2 \cdot 10^{20}$ neutrons/cm^2, the concentration of helium in the body of the sample amounts to $\sim 4.5 \cdot 10^{-5}$ at.%. Thus, with this concentration of helium and a temperature of the grain-boundary internal-friction maximum of nickel of

$T_n = 450°C$, adsorption saturation of the grain boundaries originates. The binding energy of helium with the grain-boundary collectors at this temperature, calculated by relation (2), amounts to (0.93 ± 0.04) eV, and the principal error of the calculated binding energy originates due to the error in the measurement of T_n, equal to $\pm 10°C$, since a change of the calculated concentration of helium even by a factor of 10 changes the value of F by > 0.01 eV. It should be noted that the value obtained for the binding energy of helium with the grain boundaries exceeds the value found for atoms of other impurities [3].

LITERATURE CITED

1. V. F. Zelenskii and I. M. Neklyudov, Problems of Nuclear Science and Technology, Series Physics of Radiation Damage and Radiation Material Behavior [in Russian], No. 5(19), p. 3 (1981).
2. G. Gleiter and B. Chalmers, Large-Angled Grain Boundaries [Russian translation], Mir, Moscow (1975).
3. E. É. Glinkman and Yu. V. Piguzov, in: Analytical Possibilities of the Method of Internal Friction [in Russian], Nauka, Moscow (1973), p. 75.
4. É. U. Grinik, V. S. Karasev, and M. I. Paliokha, Problems, of Nuclear Science and Technology, Series Nuclear Material Behavior [in Russian], No. 1(1) (1978), p. 25.
5. I. K. Kikoin, Tables of Physical Quantities [in Russian], Atomizdat, Moscow (1976).

How To Comply With The New Copyright Law

Participation in the Copyright Clearance Center (CCC) assures you of legal photocopying at the moment of need.

Libraries everywhere have found the easy way to fill photocopy requests legally and instantly, without the need to seek permissions, from more than 3000 key publications in business, science, humanities, and social science. You can:

Fill requests for multiple copies, interlibrary loan (beyond the CONTU guidelines), and reserve desk without fear of copyright infringement.

Supply copies from CCC-registered publications simply and easily.

The Copyright Clearance Center is your one-stop place for on-the-spot clearance to photocopy for internal use.

Its flexible reporting system accepts photocopying reports and returns an itemized invoice. You send only one convenient payment. CCC distributes it to the many publishers whose works you need.

And, you need not keep any records, the CCC computer will do it for you. Register now with the CCC and you will never again have to decline a photocopy request or wonder about compliance with the law for any publication participating in the CCC.

To register or for more information, just contact:

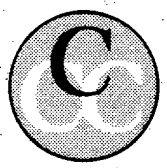

Copyright Clearance Center
21 Congress Street
Salem, Massachusetts 01970
(617) 744-3350

a not-for-profit corporation

NAME _____ TITLE _____

ORGANIZATION _____

ADDRESS _____

CITY _____ STATE _____ ZIP _____

COUNTRY _____ TELEPHONE _____

CHANGING YOUR ADDRESS?

In order to receive your journal without interruption, please complete this change of address notice and forward to the Publisher, 60 days in advance, if possible.

(Please Print)

Old Address:

name

address

city

state (or country) zip code

New Address

name

address

city

state (or country) zip code

date new address effective

name of journal

THE LANGUAGE OF SCIENCE
Plenum
PUBLISHING CORPORATION

233 Spring Street, New York, New York 10013

Declassified and Approved For Release 2013/02/06 : CIA-RDP10-02196R000300020006-4

MEASUREMENT TECHNIQUES
Izmeritel'naya Tekhnika
Vol. 25, 1982 (12 issues) $400

MECHANICS OF COMPOSITE MATERIALS
Mekhanika Kompozitnykh Materialov
Vol. 18, 1982 (6 issues) $330

METAL SCIENCE AND HEAT TREATMENT
Metallovedenie i Termicheskaya Obrabotka Metallov
Vol. 24, 1982 (12 issues) $420

METALLURGIST
Metallurg
Vol. 26, 1982 (12 issues) $435

PROBLEMS OF INFORMATION TRANSMISSION
Problemy Peredachi Informatsii
Vol. 18, 1982 (4 issues) $320

PROGRAMMING AND COMPUTER SOFTWARE
Programmirovanie
Vol. 8, 1982 (6 issues) $135

PROTECTION OF METALS
Zashchita Metallov
Vol. 18, 1982 (6 issues) $380

RADIOPHYSICS AND QUANTUM ELECTRONICS
Izvestiya Vysshikh Uchebnykh Zavedenii, Radiofizika
Vol. 25, 1982 (12 issues) $400

REFRACTORIES
Ogneupory
Vol. 23, 1982 (12 issues) $380

SIBERIAN MATHEMATICAL JOURNAL
Sibirskii Matematicheskii Zhurnal
Vol. 23, 1982 (6 issues) $495

SOIL MECHANICS AND FOUNDATION ENGINEERING
Osnovaniya, Fundamenty i Mekhanika Gruntov
Vol. 19, 1982 (6 issues) $380

SOLAR SYSTEM RESEARCH
Astronomicheskii Vestnik
Vol. 16, 1982 (4 issues) $275

SOVIET APPLIED MECHANICS
Prikladnaya Mekhanika
Vol. 18, 1982 (12 issues) $400

SOVIET ATOMIC ENERGY
Atomnaya Énergiya
Vols. 52–53 (12 issues) $440

SOVIET JOURNAL OF GLASS PHYSICS AND CHEMISTRY
Fizika i Khimiya Stekla
Vol. 8, 1982 (6 issues) $175

SOVIET JOURNAL OF NONDESTRUCTIVE TESTING
Defektoskopiya
Vol. 18, 1982 (12 issues) $485

SOVIET MATERIALS SCIENCE
Fiziko-khimicheskaya Mekhanika Materialov
Vol. 18, 1982 (6 issues) $345

SOVIET MICROELECTRONICS
Mikroélektronika
Vol. 11, 1982 (6 issues) $195

SOVIET MINING SCIENCE
Fiziko-tekhnicheskie Problemy Razrabotki Poleznykh Iskopaemykh
Vol. 18, 1982 (6 issues) $420

SOVIET PHYSICS JOURNAL
Izvestiya Vysshikh Uchebnykh Zavedenii, Fizika
Vol. 25, 1982 (12 issues) $400

SOVIET POWDER METALLURGY AND METAL CERAMICS
Poroshkovaya Metallurgiya
Vol. 21, 1982 (12 issues) $435

STRENGTH OF MATERIALS
Problemy Prochnosti
Vol. 14, 1982 (12 issues) $495

THEORETICAL AND MATHEMATICAL PHYSICS
Teoreticheskaya i Matematicheskaya Fizika
Vols. 50–53, 1982 (12 issues) $380

UKRAINIAN MATHEMATICAL JOURNAL
Ukrainskii Matematicheskii Zhurnal
Vol. 34, 1982 (6 issues) $380

Send for Your Free Examination Copy

Plenum Publishing Corporation, 233 Spring St., New York, N.Y. 10013
In United Kingdom: 88/90 Middlesex St., London E1 7EZ, England
Prices slightly higher outside the U.S. Prices subject to change without notice.

RUSSIAN JOURNALS IN THE PHYSICAL AND MATHEMATICAL SCIENCES

AVAILABLE IN ENGLISH TRANSLATION

ALGEBRA AND LOGIC
Algebra i Logika
Vol. 21, 1982 (6 issues) $270

ASTROPHYSICS
Astrofizika
Vol. 18, 1982 (4 issues) $320

AUTOMATION AND REMOTE CONTROL
Avtomatika i Telemekhanika
Vol. 43, 1982 (24 issues) issues) $495

COMBUSTION, EXPLOSION, AND SHOCK WAVES
Fizika Goreniya i Vzryva
Vol. 18, 1982 (6 issues) $345

COSMIC RESEARCH
Kosmicheskie Issledovaniya
Vol. 20, 1982 (6 issues) $425

CYBERNETICS
Kibernetika
Vol. 18, 1982 (6 issues) $345

DIFFERENTIAL EQUATIONS
Differentsial'nye Uravneniya
Vol. 18, 1982 (12 issues) $395

DOKLADY BIOPHYSICS
Doklady Akademii Nauk SSSR
Vols. 262–267, 1982 (2 issues) $145

FLUID DYNAMICS
Izvestiya Akademii Nauk SSSR, Mekhanika Zhidkosti i Gaza
Vol. 17, 1982 (6 issues) $380

FUNCTIONAL ANALYSIS AND ITS APPLICATIONS
Funktsional'nyi Analiz i Ego Prilozheniya
Vol. 16, 1982 (4 issues) $320

GLASS AND CERAMICS
Steklo i Keramika
Vol. 39, 1982 (6 issues) $460

HIGH TEMPERATURE
Teplofizika Vysokikh Temperatur
Vol. 20, 1982 (6 issues) $400

HYDROTECHNICAL CONSTRUCTION
Gidrotekhnicheskoe Stroitel'stvo
Vol. 16, 1982 (12 issues) $305

INDUSTRIAL LABORATORY
Zavodskaya Laboratoriya
Vol. 48, 1982 (12 issues) $400

INSTRUMENTS AND EXPERIMENTAL TECHNIQUES
Pribory i Tekhnika Eksperimenta
Vol. 25, 1982 (12 issues) $460

JOURNAL OF APPLIED MECHANICS AND TECHNICAL PHYSICS
Zhurnal Prikladnoi Mekhaniki i Tekhnicheskoi Fiziki
Vol. 23, 1982 (6 issues) $420

JOURNAL OF APPLIED SPECTROSCOPY
Zhurnal Prikladnoi Spektroskopii
Vols. 36–37 (12 issues) $420

JOURNAL OF ENGINEERING PHYSICS
Inzhenerno-fizicheskii Zhurnal
Vols. 42–43, 1982 (12 issues) $420

JOURNAL OF SOVIET LASER RESEARCH
A translation of articles based on the best Soviet research in the field of lasers
Vol. 3, 1982 (4 issues) $95

JOURNAL OF SOVIET MATHEMATICS
A translation of Itogi Nauki i Tekhniki and *Zapiski Nauchnykh Seminarov Leningradskogo Otdeleniya Matematicheskogo Instituta im. V. A. Steklova AN SSSR*
Vols. 18–20, 1982 (18 issues) $680

LITHOLOGY AND MINERAL RESOURCES
Litologiya i Poleznye Iskopaemye
Vol. 17, 1982 (6 issues) $420

LITHUANIAN MATHEMATICAL JOURNAL
Litovskii Matematicheskii Sbornik
Vol. 22, 1982 (4 issues) $205

MAGNETOHYDRODYNAMICS
Magnitnaya Gidrodinamika
Vol. 18, 1982 (4 issues) $325

MATHEMATICAL NOTES
Matematicheskie Zametki
Vols. 31–32, 1982 (12 issues) $400

continued on inside back cover

Declassified and Approved For Release 2013/02/06 : CIA-RDP10-02196R000300020006-4